Halme, Janne; Boschloo, Gerrit; Hagfeldt, Anders; Lund, Peter

Spectral characteristics of light harvesting, electron injection, and steady-state charge collection in pressed TiO2 dye solar cells

Published in:
Journal of Physical Chemistry C

DOI:
10.1021/jp711245f

Published: 10/04/2008

Document Version
Peer reviewed version

Please cite the original version:
Halme, J., Boschloo, G., Hagfeldt, A., & Lund, P. (2008). Spectral characteristics of light harvesting, electron injection, and steady-state charge collection in pressed TiO2 dye solar cells. *Journal of Physical Chemistry C*, *112*(14), 5623-5637. https://doi.org/10.1021/jp711245f

Spectral characteristics of light harvesting, electron injection, and steady state charge collection in pressed TiO_2 dye solar cells

Janne Halme,[*,†] *Gerrit Boschloo,*[‡] *Anders Hagfeldt,*[‡] *Peter Lund*[†]

Laboratory of Advanced Energy Systems, Department of Engineering Physics and Mathematics, Helsinki University of Technology, P.O. BOX 5100, FIN-02015 TKK, Finland, and Center of Molecular Devices, Department of Chemistry, Physical Chemistry, Royal Institute of Technology (KTH), Teknikringen 30, SE-10044 Stockholm, Sweden

Tel.: +35894513217, Fax: +35894513195, E-mail: janne.halme@tkk.fi

Title running head: Spectral characteristics of dye solar cells

* Corresponding author

† Helsinki University of Technology

‡ Royal Institute of Technology

ABSTRACT. The factors that limit photocurrent in dye solar cells (DSC) were studied by incident-photon-to-collected-electron efficiency (η_{IPCE}), optical, and photovoltaic measurements. Nanostructured TiO_2 photoelectrodes were prepared by compression technique on glass substrates, and half of them were given an additional heat treatment at 450 °C. The spectral absorbed-photon-to-collected-electron efficiency (η_{APCE}) of the cells was determined as a function of the photoelectrode film thickness (d) and direction of illumination and analyzed in terms of electron injection (η_{INJ}) and collection (η_{COL}) efficiency. The cells with pressed-only photoelectrodes gave significantly lower photocurrents yet their η_{APCE}, and thus η_{COL}, increased significantly with increasing d. To analyze this result quantitatively, methods were formulated based on the standard diffusion model of electron transport in nanostructured photoelectrodes for the factorization of experimental η_{APCE} data into η_{INJ} and η_{COL} parts and subsequent estimation of the effective steady state electron diffusion length (L). Consistent decoupling of η_{INJ} and η_{COL} was reached in a spectral region where electron generation rate was independent of d. η_{INJ} was low and strongly wavelength dependent, which was attributed to a poor energetic matching between dye excited states and TiO_2 acceptor states due to unfavorable electrolyte composition. L increased systematically with d in the both type of cells. In consistency with the increase of η_{IPCE} with light intensity, the result was attributed qualitative to the electron concentration dependence of L, and for a small part to decrease of film porosity with d. The diffusion model and its predictions were reviewed, and its validity in the present case was critically discussed.

KEYWORDS: Dye-sensitized, quantum efficiency, diffusion, optical, IPCE, APCE

1 Introduction

Dye-sensitized solar cells (DSC)[1,2] based on nanostructured semiconductor photoelectrodes is a promising new class of photovoltaic devices for the harvesting of solar energy. Conversion efficiencies exceeding 10 % have been obtained[3,4] and progress in long-term stability is encouraging[5-7]. In the research and development of these cells it is essential to identify factors that limit their steady state photocurrent output. A standard method for studying this experimentally is measurement of spectral incident-photon-to-collected-electron efficiency (η_{IPCE}) that contains information on the partial quantum efficiencies of the photocurrent generating processes of the cell: the light harvesting (η_{LH}), electron injection (η_{INJ}), and charge collection efficiency (η_{COL}) (Figure 1):

$$\eta_{\mathrm{IPCE}}(\lambda) = \frac{i_{\mathrm{SC}}(\lambda)}{q\Phi(\lambda)} = \eta_{\mathrm{LH}}(\lambda)\eta_{\mathrm{INJ}}(\lambda)\eta_{\mathrm{COL}}(\lambda) \quad , \tag{1}$$

where i_{SC} is the short circuit (SC) current density of the cell at incident monochromatic light with wavelength λ and photon flux Φ, and q is the elementary charge. The ratio $\eta_{\mathrm{IPCE}}/\eta_{\mathrm{LH}}$ is further defined as the absorbed-photon-to-collected-electron efficiency (η_{APCE}) to mark the division of η_{IPCE} into its optical and electrical parts.

An important merit of the DSC is that for an optimal combination of cell materials and components, η_{APCE} can be practically 100 %[1,3,8] and η_{IPCE} up to ca. 85 % in the visible spectral region[9], resulting in i_{SC} over 17 mA/cm^2 at 100 mW/cm^2 solar illumination (AM1.5G)[9,10]. Yet, room still exists for improvement of the cell efficiency by enhancing i_{SC} via η_{LH}, and especially by increasing the open circuit voltage (V_{OC}) of the cell. Central

to this problem is to understand and optimize the energetic and kinetic interplay of materials at the molecular semiconductor – dye – electrolyte interface[11,12]. Recent progress has shown that optimum cell efficiency is often found as a compromise between photocurrent and voltage enhancing factors. Attempts to increase V_{OC} by retarding the interfacial electron recombination with help of various methods including co-adsorbed molecules[13-15], thin insulating oxide layers[16,17], and semiconductors with higher conduction band edge energy[18,19], are often hampered by concurrent negative impact on η_{INJ} or η_{COL}. Besides striving for ultimate efficiencies there is also keen interest towards commercial applications by developing materials and methods compatible with roll-to-roll production of DSCs on flexible plastic substrates[20-22]. In this case, photoelectrode processing is restricted to relatively low temperatures, which usually results in diminished η_{COL} and η_{INJ} due to impaired electron transport and residual organic substances in the photoelectrode film.

To facilitate systematic development and optimization of the DSC it is therefore necessary to experimentally decouple the partial quantum efficiencies in eq 1 in order to assess their relative importance. As a first step, η_{LH} can be determined by optical characterization of the cell components[8,23] and combined with η_{IPCE} measurements so as to estimate η_{APCE}. Based on η_{APCE} data, conclusions have been made on η_{INJ} or η_{COL}, under the condition that respectively η_{COL}[24-26] or η_{INJ}[27,28] is close to 100 %.

This paper presents quantitative spectral analysis of the photocurrent limiting factors of nanostructured TiO_2 DSC prepared by the compression technique[29] on glass substrates. The spectral absorbed-photon-to-collected-electron efficiency (η_{APCE}) of the cells is determined as a function of the photoelectrode film thickness (d) and direction of

illumination by combining experimental η_{IPCE} and optical data. The results are analyzed in terms of the standard diffusion model for electron generation, transport and recombination in nanostructured photoelectrodes[28]. To support the discussion in the paper, the diffusion model and its predictions are reviewed in Appendix A. In Appendix B, the model is used to formulate two methods for the experimental factorization of the spectral steady state η_{APCE} into its η_{INJ} and η_{COL} parts in the general case when both η_{COL} and η_{INJ} are less than 100 % and wavelength dependent. By applying the methods to the η_{APCE} data we make a quantitative comparison with the diffusion model and obtain estimates for effective electron diffusion length (L) as a function of d.

2 Experimental Methods

2.1 TiO_2 photoelectrode preparation

Nanostructured TiO_2 films were prepared with the press technique[29]. A 20 wt-% suspension of TiO_2 nanoparticles (P25, Degussa) in ethanol (99.5 %) was mixed and stirred for several days in a closed glass bottle. Ca. 35 cm^2 TiO_2 films were deposited on FTO-coated glass substrates (TEC8, Pilkington) by spreading the suspension with a glass rod using tape as a spacer. The film thickness was adjusted to 3 – 22 μm by repeating 1 – 6 times deposition, drying, and mild pressing at a 100 kg/cm^2. This prevented cracking and peeling of the thickest films. The large films were patterned to a matrix of 4 mm x 6 mm films by scraping of excess TiO_2, and then cut to individual electrodes. The films were pressed at 1000 kg/cm^2 between stainless steel plates in a hydraulic press using aluminum foil to prevent adhesion to the press plates. Half of the films were sintered at 450 ºC for 1 h (called hereafter “S type”) and the others were used as such (“P type”).

The TiO_2 films were dyed in 0.3 mM solution of N719 dye (Ruthenium 535-bisTBA by Solaronix) in ethanol (99.5 %) for 64 h in the dark at room temperature and used as photoelectrodes in, correspondingly, S and P type solar cells.

Efforts were taken to limit as far as possible differences between the S and P type cells to those in the TiO_2 films induced by the sintering step. The TiO_2 powder and the substrates were heated at 450 ºC for 1 h prior to the film deposition. Ethanol was used both in the TiO_2 suspension and the dye-bath to avoid differences in solvent residuals.

For optical measurements, TiO_2 films were prepared on transparent 135 μm thick microscope cover glasses using the same methods. In this case adhesion of the film on the glass during compression at 1000 kg/cm^2 was preserved by facing the TiO_2 film with an ITO coated PET plastic foil instead of an aluminum foil. The films sustained sintering intact. Four P type and five S type films of different thickness (3.2 – 23 μm) were prepared and dyed in a 0.3 mM solution of N719 in ethanol (99.5%) for 17 hours in the dark at room temperature.

2.2 Solar cell preparation

A series of DSCs with conventional sandwich type configuration were prepared using the dyed P and S type TiO_2 films. The counter electrode was thermally platinized TEC8[30] and 60 μm thick Surlyn 1702 hotmelt was used as spacer and sealant. The electrolyte consisted of 0.6 M hexylmethylimidazodiumiodide, 0.05 M I_2 and 0.5 M tert-butylpyridine (TBP) in 3-methoxypropionitrile (3-MPN). After preparation the cells were let to cure in the dark for more than five days before measurements. Both S and P type series consisted of 24 cells in six thickness groups.

2.3 Film thickness and porosity

The thickness, area and volume of the TiO_2 films were measured with a stylus profilometer (Dektak 3M or 6M, Veeco). Samples for porosity measurements were selected from the same batch as used for the solar cells. The porosity was calculated based on the mass, volume and density of the TiO_2 film that was assumed to be 70 % anatase and 30 % rutile. The film mass was determined by scraping off the TiO_2 from the substrate with a scalpel and weighting the resulting powder with a microbalance (Mettler M3, resolution 1 μg). Thin microscope cover glasses were used as substrates for accurate collection and handling of the 0.08 – 1.1 mg powder samples.

2.4 Optical measurements

Quantitative in-situ measurement of the light harvesting efficiency of complete dye solar cells is complicated because of light scattering by the TiO_2 film and absorption by the other cell components. We followed thus the approach by Tachibana et al.[23] and estimated η_{LH} based on ex-situ reflectance and transmittance measurements of the dyed TiO_2 films and the other cell components.

Spectral reflectance (R) and transmittance (T) was measured with an Ocean Optics HR-2000 fiber optic UV-VIS spectrometer coupled with a DH-2000-BAL Deuterium-Halogen light source and an external 50 mm diameter integrating sphere with an 8 mm aperture diameter. The optical samples were faced with a microscope cover glass and the space in between was filled with 3-MPN. Leakage of scattered light[23,31] resulted in overestimation of the measured R and T, corresponding to an apparent (bias) background absorptance of 2 – 6 % at $\lambda > 850$ nm, and was corrected for by assuming equal loss

fraction in the nearly symmetrical R and T measurement geometries. The data were further corrected for the reflectance by the extra air/cover-glass interface, whereas reflectance by the glass/3-MPN interface, as well as absorption by the glass slide, 3-MPN, and bare TiO_2 films was negligible in the wavelength region of interest.

2.5 Estimation of light harvesting efficiency

To facilitate quantitative estimation of solar cell η_{LH}, control experiments were necessary to account for different dye concentration in the solar cell and optical measurements. Relative volumetric dye concentration in TiO_2 films was determined by desorbing the dye into 10 mM aqueous NaOH solution of known volume, measuring the peak absorbance (near 500 nm) of the solution by UV-VIS spectrometry and scaling the data with film volume. Data from S type films were taken as representative, since P type films detached rapidly into the desorption solution modifying its absorbance via light scattering. In the solar cells, dye concentration was nearly independent of film thickness, whereas in the optical samples it decreased by about 30 % as the thickness increased from 3 μm to 20 μm, most likely due to the shorter dying period (17 h vs. 64 h). In both cases, the dye concentration in the thinnest films was equal and ca. 0.29 $mmol \cdot cm^{-3}$ per geometric volume of the film, using molar extinction coefficient of the dye in basic aqueous solutions of $12.5 \cdot 10^3$ $cm^{-1}M^{-1}$.

The solar cell η_{LH} was calculated based on the optical data using eqs A13 and A14 and correcting for the dye concentration difference. Sensitivity analysis confirmed that uncertainties related to this correction were insignificant with respect to the main results of the paper. Values $\varepsilon = 2$, corresponding to a semi-isotropic diffuse light flux, and $P =$

0.55 were used to account for light absorption by the pore electrolyte (see Appendix A). Thickness differences between the optical and solar cell films were accounted for by linear interpolation of data.

2.6 IPCE measurements

Solar cell η_{IPCE} was measured at the short circuit condition using a computerized setup consisting of a xenon arc lamp (300 W Cermax, ILC Technology) coupled to a 1/8 m monochromator (CVI Digikröm CM 110), a Keithley 2400 source meter and a Newport 1830-C power meter with a 818-UV detector head. Light intensity and photon flux incident on the cell was 0.16 – 0.43 mW/cm^2 and $3.5 \cdot 10^{18}$ – $17 \cdot 10^{18}$ m^{-2}s^{-1} respectively in the wavelength region 450 – 800 nm, and 0.27 mW/cm^2 and $8.8 \cdot 10^{18}$ m^{-2}s^{-1} respectively at λ = 640 nm. Measurements were taken in the absence of bias light with the monochromatic light incident on the cells through a 3 mm x 4 mm aperture either from the photoelectrode (PE illumination) or counter electrode (CE illumination) side. The light intensity dependence of η_{IPCE} was measured at 0.47 mW/cm^2 – 42 mW/cm^2 using a red LED (Lumiled Luxeon Star 1W, λ_{peak} = 639 nm, FWHM = 21 nm, FWTM = 50 nm) as the light source.

2.7 Photovoltaic measurements

Photovoltaic measurements were carried out at 100 mW/cm^2 (1 sun) white light intensity from a sulfur lamp (Lightdrive 1000 from Fusion Lighting). Current – voltage (IV) curves were measured with a Keithley 2400 source meter sweeping the cell voltage three cycles between the short circuit and open circuit conditions, and showed negligible hysteresis. The error margins in the IV parameters indicate the standard deviation of

current, reflecting the temporal instability of the light intensity (peak-to-peak 5 %, standard deviation 1 %) and cell temperature (not controlled). The IV data are related to the geometric area of the TiO_2 film.

3 Results and discussion

3.1 TiO_2 film thickness and porosity

Nanostructured TiO_2 films of even quality and well defined thickness were necessary for the present study, which required optimization of the film deposition technique. The tape frame method commonly used for depositing single electrode films was inadequate as it gave uneven films due to surface tension of the particle suspension. The problem was solved by depositing large area films that were pattered and cut into individual electrodes prior to final pressing. As a result, large number of TiO_2 electrodes with roughly equal and uniform thickness and sharp edges were obtained easily in parallel (inset in Figure 2). The flat film profile indicates that the compression pressure was uniform and lateral variations in the film quality are likely small.

Fundamental experimental investigation of the relation between photoelectrode film thickness (d) and cell performance requires that the film quality is d-independent. We used porosity measurements to check this. Figure 2 shows that the porosity decreases with d from about 54 % at d = 3 μm to about 45 % at d = 15 μm. The final porosity of pressed TiO_2 powder films depends on the applied pressure[29,32]. The reason for the decline of porosity with d may thus be that a fraction of the compression force was exerted on the substrate instead of the film, this fraction being larger for thinner films. As discussed later in detail, this porosity variation seems to be small enough as not to

significantly interfere with the interpretation of the results of this paper. The porosity of the S and P type films was equal in as much as the film thickness was not affected by sintering.

3.2 Optical data and light harvesting efficiency

No significant difference in optical properties was found between the dyed S and P type films. An immediate conclusion is that the both type of cells had equal η_{LH}. Optical data from the both type of films are therefore combined in the following analysis.

Figures 3a-c show the reflectance (R), transmittance (T) and absorptance (A) spectra of the dyed TiO_2 optical sample films of different thickness. The light scattering magnitude of the films increases with d, as evidenced by the increase of R at $\lambda > 750$ nm where the dye absorbs weakly or negligibly. At λ = 450 – 700 nm, R is only 1 – 4 % and independent of d, meaning that the strong light absorption by the dye effectively suppresses back scattering of light from the bulk of the film. For comparison, R was about 30 % at 600 nm in the thickest films before dye-adsorption. At $\lambda = 450 – 550$ nm, T is close to zero for $d > 14$ μm, and accordingly, A saturates to ca. 97 % being limited only by R. The effect of increasing d is most significant in the weakly absorbed long wavelengths, and reveals that the N719 dye, attached to TiO_2 and surrounded by the electrolyte solvent, can absorbs photons up to about 820 nm, in agreement with previous results[23]. The absorption maximum of the adsorbed dye is at $\lambda \approx 530$ nm.

Light absorption by the electrolyte extends up to 650 nm and is notable below 520 nm (Figure 3d). $T = 80 – 88$ % at $\lambda = 450 – 800$ nm for the FTO-glass substrates, but ca. 4 –

5 %-units lower for the counter electrode, due mainly to light absorption by the platinum catalyst.

Figures 3e-f show the solar cell η_{LH} estimated based on the optical data by eqs A13 and A14. Optical losses limit the maximum η_{LH} to about 86 % and 79 % at the PE and CE illumination respectively. Light absorption by the electrolyte in the pores of the TiO_2 film (data not shown) is small compared to the effect of the bulk electrolyte at the CE illumination. The data display light attenuation characterized by an effective Napierian spectral absorption coefficient that increases with d (data not shown). This may be due to multiple scattering effects that amplify with increasing d. Application of light scattering particles or add-layers is known to be an effective method to boost the η_{LH}[9,33] and a similar effect may be present here.

Finally, we note that the optical data were consistent with visual inspection of the color and transparence of the solar cells against bright background light. No difference could be distinguished between the S and P type cells, and the transparence was similar for $d >$ 14 μm.

3.3 Photovoltaic performance

Figure 4 shows the short circuit current density (i_{SC}) and energy conversion efficiency (η) of the solar cells at 100 mW/cm^2 light intensity. In agreement with previous results[34], the S type cells display overall higher η compared to the P type cells. In the S cells, i_{SC} has an apparent maximum of 9.7 mA/cm^2 at d = 17 μm, whereas in the P cells, i_{SC} increases over the whole thickness range. For $d <$ 20 μm, the S cells give more than twice as high i_{SC} as the P cells. The open circuit voltage (V_{OC}) of the S cells decreases from

0.84 V at d = 3 μm to 0.77 V at d = 23 μm, whereas in the P cells it is systematically ca. 30 – 50 mV lower (data not shown). The fill factor (FF) is 0.68 – 0.73 in the S cells, and again, systematically ca. 0.02 – 0.04 smaller in the P cells (data not shown).

For the S type cells, the maximum i_{SC} is lower than in previous studies that reported 11.9 mA/cm^2 at similar conditions[34]. On the other hand, the V_{OC} and FF of the S cells are higher than the previously reported[21] $V_{OC} \leq 0.72$ V and $FF \leq 0.61$, and as a result, the maximum η falls in the same range[34]. The P type cells lag however somewhat behind the previous results in terms of all IV parameters[21,29,35,36].

3.4 IPCE data

The present paper builds on the quantitative combination of estimated η_{LH} with measured η_{IPCE} so as to determine the spectral η_{APCE}. In the following, we take a brief look on the experimental η_{IPCE} data and make some initial observations, but postpone detailed discussions to the analysis of the η_{APCE} data later on.

Illumination from the PE side

Figures 5a-c and 6a-c show the η_{IPCE} data at the PE illumination. The two cell types have some common characteristics. The η_{IPCE} spectra peak near 540 nm in accordance with the absorption maximum of the dyed TiO_2 films. Unlike η_{LH}, η_{IPCE} is negligibly small for $\lambda > 800$ nm. Similar to η_{LH}, η_{IPCE} increases with d, the effect being most significant in the longer wavelengths. A distinctive feature is that the η_{IPCE} is relatively low even for the thickest films. The maximum η_{IPCE} is ca. 35 % in the S films and ca. 23 % in the P cells, compared to the maximum η_{LH} of ca. 83 %. This is consistent with the

relatively low i_{SC} obtained in the photovoltaic measurements and shows that the both type of cells suffer from substantially low η_{APCE}.

The S cells display generally higher η_{IPCE} than the P cells at given d and λ. Looking for a moment at the η_{IPCE} data at 535 nm (Figures 5a-c and 6a-c), the P cells yield only 35 % of the η_{IPCE} of the S cells at $d \approx 3$ μm, but this ratio increases to 78 % at $d \approx 22$ μm, meaning that the P cells benefit more from the photoelectrode thickness increase. The η_{IPCE} of the S cells reaches maximum at $d \approx 17$ μm, whereas the η_{IPCE} of the P cells increases over the whole d range, even though the η_{LH} saturates to the maximum already at $d \approx 8$ μm (Figure 3f). For the both cell types, the trend of the η_{IPCE} vs. d at 535 nm is thus similar to the i_{SC} vs. d in the photovoltaic measurements (Figure 4).

The η_{IPCE} spectra broaden with increasing d, but the effect is markedly weaker in the P cells than in the S cells (Figures 5c and 6c). Interestingly, the normalized η_{IPCE} spectra overlap accurately within each film thickness group, which means that the small random sample-to-sample variation in η_{IPCE} is wavelength-independent by nature.

Illumination from the CE side

Figures 5d-f and 6d-f present the η_{IPCE} data at the CE illumination. The effect of the reversed direction of illumination is most dramatic in the P cells. At strongly absorbed λ, η_{IPCE} decreases rapidly to negligibly small values when d increases. As a consequence, the η_{IPCE} peak shifts towards longer wavelengths. This indicates clearly that the P cells suffer considerably from recombination losses, i.e. low η_{COL}[28,37,38]. The S cells follow similar but much less pronounced trend, indicating significantly higher η_{COL}.

Light intensity dependence of η_{IPCE}

Figure 7 shows the light intensity dependence of η_{IPCE} at λ = 640 nm. Both types of cells show clear increase of η_{IPCE} with intensity up to ca. 10 mW/cm^2, this being more pronounced in the P cells. Since η_{LH} and η_{INJ} can be taken independent of intensity for sufficiently low intensities, the light intensity dependence of η_{IPCE}[39-41] can be attributed to η_{COL}, and has been explained by an electron diffusion length that is an increasing function of electron concentration[38,39]. We will return to this point later in the paper.

The decline of the η_{IPCE} at the high light intensities is likely related to mass transport limitations at the photoelectrode. The highest current density in these measurements was ca. 6 mA/cm^2 for the S type cells, which is much lower than the 10 mA/cm^2 reached at photovoltaic measurements. This indicates that, instead of mass transport limitations at the counter electrode, the η_{IPCE} decline is likely due to accumulation of triiodide at the photoelectrode, which enhances electron recombination and lowers η_{COL}. In addition, decline of iodide concentration with increasing current may retard dye regeneration and lower η_{INJ}. These effects are also the likely reason for decrease of i_{SC} and thus the conversion efficiency with d for d > 18 μm observed for the S cells in the photovoltaic measurements at high light intensity (Figure 4).

3.5 APCE data

Figures 8 and 9 present the η_{APCE} data calculated based on the estimated η_{LH} and measured η_{IPCE}. We restrict the analysis and discussion of the η_{APCE} data to λ > 520 nm. Below this wavelength, the data at the CE illumination are considered to be less accurate

due to uncertainly in the thickness of the strongly absorbing bulk electrolyte layer, which was determined by the slightly compressible hot-melt sealant.

Illumination from the PE side

Figures 8a-c and 9a-c display the η_{APCE} data at the PE illumination. Quite remarkably, in the P cells η_{APCE} increases drastically with d over the whole thickness and wavelength ranges, whereas in the S cells it is almost independent of d at all wavelengths. Similar to the η_{IPCE} and η_{LH} spectra, the η_{APCE} spectra display a peak near 535 nm. With constant d and above the peak wavelength, η_{APCE} decreases steeply towards longer wavelengths in the both type of cells. Note also that the spectral shape of the η_{APCE} is strikingly insensitive to d in the both type of cells except for the slight broadening in the P cells with one layer of TiO_2.

Illumination from the CE side

At the CE illumination, the η_{APCE} data is sensitive both to light wavelength and photoelectrode thickness (Figures 8d-f and 9d-f). At the short wavelengths, η_{APCE} decreases steeply with d in the P cells, this effect being smaller but non-negligible in the S cells. At the long wavelengths a small increase of η_{APCE} with d is observed in the both type of cells similarly to what was found at the PE illumination. The wavelength dependence of η_{APCE} at constant d displays similar features as the η_{IPCE} spectra, including the shift of the peak towards longer wavelengths with increasing d. Similar but smaller effect is found in the S cells that show broadening of the η_{APCE} spectra without peak shifting.

3.6 Qualitative comparison to the standard diffusion model

As in previous studies[28,37,38], the main qualitative features of the η_{APCE} data can be understood in terms of the standard diffusion model and its predictions, summarized in Appendix A and Figure 14a. The insensitivity of η_{APCE} to d in the S cells at the PE illumination can be attributed to a high η_{COL}. The decline of η_{APCE} at the CE illumination compared to the PE illumination indicates recombination losses due to insufficiently long electron diffusion length L, this being here more severe in the P type cells. The spectral sensitivity of this decline, and the resulting red shift of the η_{APCE} peak in the P cells, originates from the intimate relation between light attenuation and electron generation profile in the photoelectrode film.

As a striking exception, the significant increase of η_{APCE} with d in the P cells at the PE illumination is clearly in contrast with the diffusion model if L is assumed constant (cf. Figure 14a). Rather, it indicates that L is an increasing function of d. This result prompted us to perform quantitative analysis of the η_{APCE} data by the standard diffusion model, and this is the topic for the rest of the paper. However, it is important to note that in the case of the P type cells our main conclusion, the significant increase of L with increasing d, can be made qualitatively already at this point: Since the S and P cell types were optically identical and their η_{INJ} should be d-independent, the d-dependence of their short circuit photocurrent reflects differences in the η_{COL} only. Should the lower i_{SC} and η_{IPCE} of the P type cells be due to a shorter *constant* L, we would expect their photocurrent to be similar to the S cells for small d and saturate to an L-limited value as d increases. Quite the contrary, the photocurrent of the P cells increases over the whole experimental thickness

range as noted in the preceding sections (Figures 4, 5b, and 7a). The increase of η_{APCE} with d further clarifies the result.

The analysis in the rest of the paper brings this discussion to a quantitative basis and extends it to the S type cells, yielding similar results.

3.7 Decoupling of η_{INJ} and η_{COL} and estimation of *L*

In Appendix B we formulate methods implied by the standard diffusion model for the quantification of the spectral η_{INJ} and η_{COL} and estimation of the L based on η_{APCE} data. In the following, we apply these methods to the present experimental data and discuss the results and limitations thereof.

The S type cells with thinnest photoelectrodes display high η_{COL}

According to the diffusion model, close to equal η_{APCE} for opposite illumination directions is a fingerprint of $\eta_{COL} \approx 100$ %. This condition is satisfied rather well in the S type cells with the thinnest photoelectrodes that have $\eta_{APCE,CE}/\eta_{APCE,PE} > 0.92$ for $\lambda > 535$ nm (Figure 12a). Furthermore, the η_{APCE} is relatively insensitive to d at the PE illumination as expected by the diffusion model for $L > 2d$ and constant η_{INJ}. Hence, as a reasonable initial estimate the η_{INJ} of the S type cells can be taken equal to their η_{APCE} at the PE illumination (Figure 9a).

Extrapolation of η_{APCE} to $d = 0$

The diffusion model implies that η_{INJ} should in principle be obtained by extrapolating η_{APCE} data to $d = 0$, since according to the model $\eta_{COL} = 100$ % at this limit. In the

present case however, quantitative estimation of η_{INJ} in this way is clearly not possible since η_{APCE} is an increasing function of d at the PE illumination (Figures 8b and 9b). To be consistent with the d-dependent data, η_{INJ} must be higher than the highest measured η_{APCE} at each wavelength since by definition, $\eta_{COL} \leq 100$ %. Hence, for these cells the limit of η_{APCE} at $d = 0$ is an underestimation of their true η_{INJ}.

It is nevertheless interesting to investigate the spectral shape of η_{APCE} extrapolated to $d = 0$, and this data is shown in Figure 10. The S type cells yield equal zero-thickness-η_{APCE} for the both illumination directions, which as such is in agreement with the diffusion model. Very similar spectral shape is observed in the P cells at the PE illumination. This indicates that η_{INJ} has similar spectral properties in the both type of cells, as is expected considering the measures taken in the cell preparation to equalize the TiO_2 surface properties. The peak value of η_{APCE} at $d \rightarrow 0$ is however much lower in the P cells as evident already from the Figures 8b and 9b.

Despite the failure of the extrapolation to yield correct peak value of η_{INJ} we continue with the method in order to make a spectral comparison of the η_{APCE} data with the diffusion model in terms of η_{COL}. For this, we assume that the η_{INJ} is equal in the both type of cells, has the spectral shape of Figure 10 and a peak value of 49 % near $\lambda = 535$ nm. This particular value was chosen based on the η_{APCE}-ratio method discussed below, but our conclusions are not particularly sensitive to this choice as it does not affect the d-dependence of the data. Using this $\eta_{INJ}(\lambda)$ estimate, $\eta_{COL}(\lambda,d)$ is readily calculated from eq A2 based on the $\eta_{APCE}(\lambda,d)$ data. As an example, we show the results for the P type cells in Figure 11. To contrast the $\eta_{COL}(\lambda,d)$ data with the diffusion model, a wavelength

independent $L(d)$ was estimated by fitting eqs A11 and A12 to the $\eta_{COL}(\lambda,d)$ data at λ = 535 nm with $\alpha(\lambda,d)$ and d fixed to their experimental values, and using L as the only free parameter. Figure 13 shows that in the P type cells the estimated L increases linearly with d at the PE illumination following a constant ratio $d/L \approx 5$. At the CE illumination, similar L vs. d trend is obtained, apart from the 5 – 6 layer films that yield lower values.

The experimental and model-fitted η_{COL} have similar spectral features, but do not match quantitatively over the whole wavelength region (Figure 11). The disagreement means that in these measurements, L varies not only with d but also with λ. This may be related to the electron concentration dependence of η_{COL}, which was evidenced by the increase of η_{IPCE} with light intensity (Figure 7a). For constant d the average electron concentration depends on the total electron generation rate given by $g(d,\lambda) = \Phi(\lambda)\eta_{INJ}(\lambda)\eta_{LH}(d,\lambda)$, where $\Phi(\lambda)$ is the incident photon flux. Due to the large spectral variation of $\eta_{INJ}(\lambda)$ in the present case, g is relatively constant (within 20 %) only in the narrow region 525 nm < λ < 575 nm for the cells with 2 – 6 layers of TiO_2. The spectral trends in the experimental η_{COL} at the longer wavelengths should thus be taken only qualitative here. The estimation of L at 535 nm is however reasonable since at this wavelength, g varies no more than 10 % for the cells with 2 – 6 layers of TiO_2, due to the rapid saturation of the η_{LH} with increasing d.

Ratio of η_{APCE} at the opposite illumination directions

The other method implied by the diffusion model for the factorization of η_{APCE} is based on the experimental value of the ratio $\eta_{APCE,CE}(\lambda,d)/\eta_{APCE,PE}(\lambda,d)$. According to eq B1, this ratio depends only on $\alpha(\lambda)$, d and L. Using the experimental data for $\alpha(\lambda,d)$ and d, L

was calculated from eq B1, and subsequently $\eta_{COL}(\lambda,d)$ from eqs A11-A12, and $\eta_{INJ}(\lambda,d)$ from eq B2. The method inherently assumes that L is independent of the illumination direction, and we further expect η_{INJ} to be independent of d.

Figure 12 presents the results of the η_{APCE}-ratio method for the S cells. The estimated $\eta_{INJ}(\lambda)$ is independent of d only within a narrow region 520 nm < λ < 580 nm, which coincides with the region of constant electron generation rate mentioned above. As d increases, $\eta_{INJ}(\lambda)$ approaches spectral shape that is strikingly similar to that in Figure 10. This is quite remarkable since the latter was obtained at the limit $d \rightarrow 0$. The reason for the d-dependence of $\eta_{INJ}(\lambda)$ for λ > 580 nm in Figure 12c is not clear for the present, but is likely due to low experimental accuracy at low η_{IPCE} in the case of $\eta_{APCE,CE}/\eta_{APCE,PE} \approx 1$. The estimated L, shown in Figure 13, increases systematically with d at all wavelengths, but should be taken valid only where $\eta_{INJ}(\lambda)$ is independent of d, such as at 535 nm where η_{INJ} = (49 ± 2) %. At this wavelength, the ratio d/L increases from 0.8 to 1.4 with d. The S cells have thus systematically much longer L compared to the P cells.

Comparison of the methods

The P cells were analyzed independently also with the η_{APCE} -ratio method. Figure 13 shows that the L estimated with this method follows closely that obtained by the extrapolation method at the CE illumination. The corresponding spectral data, given as Supporting Information, show that the estimated η_{INJ} has similar spectral features as in the S cells, but is subject to more experimental uncertainty. As in the S cells (cf. Figure 12c), the method fails at longer wavelengths, indicated by rapid increase of η_{INJ} estimate above certain wavelength that increases with increasing d. The method also fails to give

meaningful η_{INJ} estimates for the 5 and 6 layer films below 570 nm. This is most likely due to the very low $\eta_{APCE,CE}$ involved (Figure 8d), and suggests that the L estimates for the 5 and 6 layer P cells by this method, and thus likely also by the extrapolation method at the CE illumination, should be considered unreliable. For $d < 15$ μm however, both methods give systematically similar L for the P cells.

Figure 13 shows also L determined by the extrapolation method for the S cells, but the results form the two methods are not independent in this case. In the extrapolation method η_{INJ} was fixed to the mean value of η_{INJ} obtained by the η_{APCE} -ratio method for the S cells, and hence both methods give the same result for purely mathematical reasons.

The η_{APCE}-ratio method seems particularly promising for experimental factorization of $\eta_{APCE}(\lambda)$ data to $\eta_{INJ}(\lambda)$ and $\eta_{COL}(\lambda)$ parts, since it is not affected by the d-dependence of L, but can on the contrary be used to directly estimate L as a function of d. Furthermore, checking the invariance of η_{INJ} upon changing d provides a way to assess the validity of the data. However, the method seems to be affected by variation of the electron generation rate with λ, and for this reason was here valid only near the absorption maximum of the dye. The extrapolation method on the other hand was unable to give quantitative estimate for η_{INJ} due to the d-dependence of L. An important merit of this method was however that, unlike the η_{APCE}-ratio method, it yielded consistent results for the spectral shape of η_{INJ} over the whole wavelength region. In this respect, the methods are complementary to each other.

3.8 Electron injection efficiency

The low η_{INJ} peak value agrees with the modest maximum i_{SC} of ca. 10 mA/cm^2 in the S cells compared to the over 18 mA/cm^2 reached with optimized DSC at 100 mW/cm^2 AM1.5G illumination using the same dye[6]. This confirms that the photocurrent of the cells is limited mainly by inefficient electron injection. The low η_{INJ} and its steep decrease towards the longer wavelengths indicate that there is a significant mismatch between the excited state energy levels of the dye and the electron acceptor states in the TiO_2. This energy level matching is sensitive to and can be modified by the surface density and size of co-adsorbed ions and molecules[15,42-48] that upon adsorbing on the semiconductor determine the magnitude and distribution of the electrostatic potential difference across the interfacial Helmholtz layer[12,49]. If the energetic matching is sufficiently good the η_{INJ} can be close to unity[8,26] and independent of the light wavelength[8,25,50], whereas for poor matching the η_{INJ} is reduced and depends on the excitation wavelength[25,45,46,51-54]. Addition of Li^+ in the electrolyte lowers the TiO_2 conduction band energy relative to the dye energy levels, resulting in the increase of η_{INJ}, especially at longer wavelengths[13,45,55], whereas addition of TBP[13,26,52] or large cations[55] tend to have an opposite effect. The low η_{INJ} and its spectral shape in the present case can thus be attributed to absence of Li^+ and presence of large HMI^+ cations and TBP in the electrolyte. Each of these factors contributes to a high TiO_2 conduction band energy relative to the dye and redox energy levels, which is also consistent with the relatively high V_{OC} in these cells.

3.9 Increase of electron diffusion length with film thickness

The strong increase of L with d is somewhat surprising and deserves to be critically discussed. In the following, we consider whether this result could be explained by invalidity of certain assumptions and simplifications of the standard diffusion model in our experimental case.

Porosity variation

The diffusion model assumes that the structure and properties of the photoelectrode film are uniform and isotropic. While this was likely true for the individual TiO_2 films, their porosity decreased slightly with d (Figure 2). Besides modifying the volumetric density and surface area, porosity affects the electron transport properties of the TiO_2 film[32,56]. According to numerical simulation of random packing of lightly sintered spheres[57], decrease of porosity from 54 % (obtained here at d = 3 μm) to 45 % (at 15 μm) increases the average coordination number of particles from 4.6 to 5.7. According to random-walk simulations[56], this corresponds to increase of electron diffusion coefficient by 32 %. Assuming that the electron lifetime is not affected this predicts no more than 15 % larger L for the 15 μm compared to the 3 μm thick films. Only a small fraction of the experimentally observed variation of L with d (cf. Figure 13) can thus be explained by the porosity.

Concentration dependence of *L*

In the diffusion model, it is assumed that the steady state electron diffusion coefficient and lifetime are independent of the electron concentration. A large body of experimental

evidence from the past ten years shows that the D and τ measured by small amplitude dynamic techniques depend on the contrary strongly on the electron concentration[58,59], but compensate each other so that $L = (D\tau)^{1/2}$ is nearly constant[39,60]. It was recently shown by numerical modeling[61] that if the compensation is exact, the steady state IV characteristics of the cell are not affected by the concentration dependence of D and τ, and thus, eqs A11 and A12 remain valid. In reality the compensation is not perfect, but L increases with the electron concentration making η_{IPCE} vary with light intensity (Figure 7 and refs.[38-41]). According to the diffusion model, and experiments[62-64], an electron concentration profile is established in the film at the short circuit condition under illumination. As the electron generation rate increases with increasing light intensity, the concentration gradient becomes steeper, increasing the average electron concentration in the film. Similarly, increase of average electron concentration is expected when d is increased at constant light intensity, and we have also confirmed this by charge extraction experiments to be reported elsewhere. Our finding that L increases with d is thus in qualitative agreement with the diffusion model if we allow for the concentration dependence of L. Quantitative treatment of this question may be feasible by numerical modeling[61], but is beyond the scope of the present paper.

Specific recombination at the substrate – electrolyte interface

Electron transfer at the photoelectrode FTO-glass substrate – I^-/I_3^- electrolyte interface follows Butler-Volmer kinetics with extremely low exchange current density[65-67]. At the short circuit condition, the overpotential that drives this recombination reaction equals to the sum of the internal voltage losses in the cell, and is thus usually small, especially at

low light intensities. In the present case, impedance and IV measurements confirmed that the cells had very high resistance at the short circuit condition even at high light intensities. Furthermore, photoelectrodes consisting of only residual TiO_2 particles delivered ca. 0.3 – 0.6 % peak η_{IPCE} and spectra similar to the complete films. The effect of substrate mediated recombination on η_{IPCE} and i_{SC} should thus be negligible here. We note however that deposition of a compact recombination blocking layer on the photoelectrode substrate has been found to increase not only V_{OC} and FF[67-73], but in some cases also i_{SC}[68,70,72,73], suggesting that the role of this interface in working DSC may still need to be clarified.

Light scattering

The diffusion model assumes that light absorption follows Beer-Lambert law and neglects thereby effects due to light scattering. Yet, the present TiO_2 films were moderately scattering. Light scattering may modify the absorption profile and render it somewhat d-dependent. To study this point we analyzed the present optical data by a four-flux radiative transfer model[74,75], which showed that for the both illumination directions, the mean distance of light absorption from the substrate contact increased monotonously with d irrespective of the assumptions made on the unknown average optical path length and forward scattering ratio parameters. This makes light scattering an unlikely explanation for the L vs. d result.

Other effects

We can also think of many other details of the DSC function that may generally influence η_{APCE} and its d-dependence. It turns out however that all of these can be either

reasoned negligible or classified as loss factors that not only diminish η_{APCE} but also *amplify* with increasing *d*. Without going into details these include mass transport in the electrolyte: increased electron recombination due to I_3^- accumulation[76,77], decreased dye regeneration and increased recombination with the oxidized dye due to I^- depletion[76-78]; charging of the photoelectrode film and its influence on the relative energetics between TiO_2, dye and redox electrolyte. The interpretation that *L* increases with *d* appears thus to be on a relatively firm basis in this respect.

Relevance to the performance characterization of dye solar cells

The electron diffusion length is generally regarded as a key parameter in the performance optimization of DSC, with the requirement $L >> d$ for a high performance cell. The present paper shows however a practical case where the increase of the photoelectrode film thickness brings about significantly larger photocurrent improvement than what would be expected based on *L* estimated from cells with a thin photoelectrode. This result may be important for the optimization of DSCs exhibiting photocurrent limitations by low η_{COL} due for example to low-temperature preparation of the photoelectrode film.

Instead of the steady state methods discussed here, $L = (D\tau)^{1/2}$ is usually estimated based on *D* and τ measured by dynamic photocurrent and photovoltage techniques, such as intensity modulated photocurrent (IMPS) and photovoltage (IMVS) spectroscopy[39,40]. The present solar cells have also been characterized by these techniques. In qualitative consistency with the present results, *L* estimated by a standard analysis of short-circuit-IMPS and open-circuit-IMVS data at constant light intensity increased linearly with *d* in

the both type of cells; from 5 μm to 25 μm in the S cells, and from 3 μm to 18 μm in the P cells. A quantitative comparison of the steady state and dynamic L is however not feasibly here due to difference in the light intensity used and overestimation of D due to influence of electron recombination on the IMPS response of the P cells. Details of this analysis will be reported elsewhere. Considering the dynamic techniques, the quantitative estimation of the steady state η_{COL} and L should be particularly useful in cases where the transient photocurrent response is dominated by the RC time-constant of the cell, as well as for experimental verification of the dynamic electron transport theories at the limit of low frequencies or long times.

To improve the methods of this paper we suggest intensity dependent spectral η_{IPCE} measurements that would allow analysis of η_{APCE} data at constant electron generation rate over a much broader spectral range.

4 Conclusions

The η_{APCE} of dye solar cells can be determined quantitatively as a function of photoelectrode film thickness and direction of illumination by combining η_{IPCE} measurements with optical characterization of the cell components. The standard diffusion model suggests two methods for the quantitative decoupling of η_{APCE} into its wavelength-dependent η_{INJ} and η_{COL} components: The first method involves extrapolation of η_{APCE} vs. d data to $d = 0$, corresponding to the limit where $\eta_{COL} = 100$ %, and can be performed separately for the both directions of illumination. The second method involves estimation of L based on the ratio of η_{APCE} at the opposite illumination directions, and yields η_{INJ} estimates independently for each d.

The methods were applied to quantification of the η_{INJ}, η_{COL} and L of pressed nanostructured TiO_2 dye solar cells. The η_{INJ} was relatively low and strongly wavelength dependent, due to unfavorable electrolyte composition in terms of energetic matching between the dye excited states and the TiO_2 acceptor states. L increased systematically with d, and enhanced upon high temperature sintering of the TiO_2 film while preserving its d-dependence. The increase of L with d was attributed qualitatively to the electron concentration dependence of L, in consistency with the increase of η_{IPCE} with light intensity. It remains to be investigated whether this is a specific property of the pressed TiO_2 films or a fundamental characteristic of the steady state electron transport in the nanostructured photoelectrodes at short circuit conditions. The latter would have important implications to the performance optimization of DSC.

Acknowledgements

This work was financial supported by the Nordic Energy Research (Norden), under the project "Nordic PV" (J.H.). Summary of the methodology of this paper with some illustrating results was presented as a poster contribution in the 2nd International DSC Industrialization Conference, 11th – 13th September 2007, St. Gallen, Switzerland.

Supporting Information Available: Results of the η_{APCE}-ratio method for the P type cells showing the experimental $\eta_{APCE,CE}/\eta_{APCE,PE}$, and the estimated L and η_{INJ} as a function of light wavelength. This information is available via the Internet at http://pubs.acs.org.

APPENDIX A: Analytical modeling of η_{IPCE}, η_{COL} and η_{LH}

The incident-photon-to-collected-electron efficiency can be defined as a product of partial efficiencies for light harvesting $\eta_{LH}(\lambda,d)$, electron injection $\eta_{INJ}(\lambda)$, and electron collection $\eta_{COL}(\lambda,d)$

$$\eta_{IPCE}(\lambda,d)=\frac{i_{SC}(\lambda,d)}{q\Phi(\lambda)}=\eta_{LH}(\lambda,d)\eta_{INJ}(\lambda)\eta_{COL}(\lambda,d)\ , \qquad \text{(A1)}$$

where $i_{SC}(\lambda,d)$ is the short circuit current density measured at incident monochromatic light of wavelength λ and photon flux $\Phi(\lambda)$, q is the elementary charge, and d the photoelectrode film thickness. Eq A1 implies that the absorbed-photon-to-collected-electron efficiency $\eta_{APCE}(\lambda,d)$

$$\eta_{APCE}(\lambda,d)=\eta_{INJ}(\lambda)\eta_{COL}(\lambda,d)\ , \qquad \text{(A2)}$$

can be determined experimentally by combining quantitatively η_{IPCE} and $\eta_{LH}(\lambda,d)$ data. The latter can be determined by optical characterization of the cell components and a simplified optical model formulated below.

Light harvesting efficiency

For simplicity, it is assumed that the light absorption profile is exponential according to eq A6 below, and the reflectance of the film is interfacial despite the fact that it originates mainly from the light scattering in the bulk of the film. Multiple reflection of light in the

cell is neglected, as well as back reflection from the counter electrode at the PE illumination and from the photoelectrode substrate at the CE illumination. With these assumptions the light harvesting efficiency η_{LH} becomes for the PE illumination (cf. ref. 8)

$$\eta_{\mathrm{LH,PE}}(\lambda,d) = T_{\mathrm{TCO}}(\lambda)\cdot\left[1-R_{\mathrm{PE}}(\lambda,d)\right]\cdot\frac{\alpha_{\mathrm{D}}(\lambda,d)}{\alpha(\lambda,d)}\cdot\left(1-e^{-\alpha(\lambda,d)d}\right) \qquad \text{(A3)}$$

and for the CE illumination

$$\eta_{\mathrm{LH,CE}}(\lambda,d) = T_{\mathrm{CE}}(\lambda)\cdot T_{\mathrm{EL}}(\lambda,d)\cdot\left[1-R_{\mathrm{PE}}(\lambda,d)\right]\cdot\frac{\alpha_{\mathrm{D}}(\lambda,d)}{\alpha(\lambda,d)}\cdot\left(1-e^{-\alpha(\lambda,d)d}\right), \qquad \text{(A4)}$$

where $T_{\mathrm{TCO}}(\lambda)$, $T_{\mathrm{CE}}(\lambda)$ and $T_{\mathrm{EL}}(\lambda,d)$ are respectively the transmittance of the TCO-coated glass substrate of the photoelectrode, the counter electrode and the free electrolyte layer, and $R_{\mathrm{PE}}(\lambda,d)$ is the reflectance of the photoelectrode film.

Electron collection efficiency according to the standard diffusion model

The present paper shows that using the standard diffusion model of electron generation, transport and recombination in nanostructured photoelectrodes the $\eta_{\mathrm{APCE}}(\lambda,d)$ can in principle be factorized into its $\eta_{\mathrm{INJ}}(\lambda)$ and $\eta_{\mathrm{COL}}(\lambda,d)$ parts in the general case when both $\eta_{\mathrm{INJ}}(\lambda)$ and $\eta_{\mathrm{COL}}(\lambda,d)$ are unknown spectral functions. This is based on the quantitative analysis of $\eta_{\mathrm{COL}}(\lambda,d)$ data by the standard diffusion model as a function of λ, d, and the direction of illumination (see Appendix B). In the following we revisit the diffusion model and review its predictions to support the discussion in the paper.

The standard diffusion model is based on the continuity equation for electron concentration[28]:

$$D\frac{\partial^2 n}{\partial x^2} - \frac{n - n_0}{\tau} + g = 0 \quad , \tag{A5}$$

where D and τ are respectively the electron diffusion coefficient and lifetime, n the local electron density, n_0 the equilibrium electron density in the dark, g the local electron generation rate and λ the light wavelength. The position coordinate x increases towards the bulk of the photoelectrode with $x = 0$ at the film edge facing the in-coming light. The generation rate is defined by the incident photon flux Φ, the electron injection efficiency η_{INJ}, the absorption coefficient of the adsorbed dye α_D and the light attenuation by the Beer-Lambert law as

$$g(x,\lambda,d) = \Phi(\lambda)\eta_{INJ}(\lambda)\alpha_D(\lambda,d)e^{-\alpha(\lambda,d)x} \quad . \tag{A6}$$

The total Napierian spectral absorption coefficient of the electrolyte filled nanoporous film is $\alpha(\lambda,d) = \alpha_D(\lambda,d) + P\varepsilon(\lambda,d)\alpha_{EL}(\lambda)$, where $\alpha_{EL}(\lambda)$ is the absorption coefficient of the bulk electrolyte solution and P the film porosity. Light scattering is accounted for by the average optical mean path length parameter ε, and implicitly by the effective absorption coefficient α_D, allowing for their possible dependence on the photoelectrode film thickness d. When the light is incident on the cell from the photoelectrode side (PE illumination) the boundary conditions for solving eq A5 at the short circuit condition are

$n(0) = n_0$ and (A7)

$$\frac{\partial n(x)}{\partial x} = 0 \qquad \text{at } x = d. \tag{A8}$$

For the opposite direction of light (CE illumination), x = 0 at the counter electrode facing edge of the film, and the boundary conditions are

$n(d) = n_0$ and (A9)

$$\frac{\partial n(x)}{\partial x} = 0 \qquad \text{at } x = 0. \tag{A10}$$

The model assumes that the electron transport occurs via diffusion, the recombination reactions are first order in the electron concentration, D and τ are independent of x and $n(x)$, and at short the circuit condition, extraction of electrons at the substrate contact is fast enough to keep the excess electron concentration at the contact close to the dark equilibrium value.

Solution of eqs A5-A10 gives expressions for the charge collection efficiency η_{COL} at the PE illumination

$$\eta_{\mathrm{COL,PE}}(\lambda,d) = \frac{\left[-L\alpha(\lambda,d)\cosh(d/L) + \sinh(d/L) + L\alpha(\lambda,d)e^{-\alpha(\lambda,d)d}\right]L\alpha(\lambda,d)}{\left(1-e^{-\alpha(\lambda,d)d}\right)\left[1-L^2\alpha(\lambda,d)^2\right]\cosh(d/L)}, \tag{A11}$$

and at the CE illumination

$$\eta_{\mathrm{COL,CE}}(\lambda,d) = \frac{\left[L\alpha(\lambda,d)\cosh(d/L) + \sinh(d/L) - L\alpha(\lambda,d)e^{\alpha(\lambda,d)d}\right]L\alpha(\lambda,d)e^{-\alpha(\lambda,d)d}}{\left(1-e^{-\alpha(\lambda,d)d}\right)\left[1-L^2\alpha(\lambda,d)^2\right]\cosh(d/L)},$$

(A12)

where $L = (D\tau)^{1/2}$ is the electron diffusion length[28]. According to eqs A11 and A12, η_{COL} is determined roughly by the mean distance from the point of electron generation to the substrate contact and its relation to L.

For given L, the decisive factor is the electron generation profile that depends on α, d, and the direction of illumination. Two special cases can be considered with this respect: uniform or highly non-uniform electron generation. For uniform generation, obtained in the limit of weak light absorption, the η_{COL} becomes

$$\eta_{COL} = \frac{\tanh(d/L)}{d/L} \qquad (1/\alpha >> d), \tag{A13}$$

and independent of the illumination direction. In the opposite case $1/\alpha << d$, corresponding to high η_{LH}, η_{COL} approaches 100 % for the PE illumination, whereas for the CE illumination it becomes

$$\eta_{COL} = \frac{1}{\cosh(d/L)} \qquad (1/\alpha << d, \text{ CE illumination}). \tag{A14}$$

In the intermediate case $1/\alpha \approx d$, η_{COL} is sensitive to α and reflects its wavelength dependence.

The main predictions of the diffusion model by eqs A11 and A12 are apparent from Figure 14a:

1. For constant L and α, η_{COL} decreases with d for the both directions of illumination.
2. For $L >> d$, η_{COL} approaches 100 %, irrespective of α and the direction of illumination.
3. For uniform electron generation, obtained in the limit of weak light absorption, η_{COL} becomes equal at the both illumination directions, irrespective of d and L.
4. For constant d and L, η_{COL} increases with α at the PE illumination, whereas at the CE illumination, the trend is opposite.

Note that at the PE illumination, η_{COL}, and especially its wavelength dependence originating from the $\alpha(\lambda)$, is sensitive to d when roughly $0.5 < d/L < 4$ (Figure 14a). For $d/L < 0.5$, $\eta_{COL} > 88$ % irrespective of the electron generation profile, whereas for $d/L > 4$ successful electron collection is fixed to a thin region close to the collecting substrate and thus, variation of d does not influence η_{COL} much. However, at the CE illumination, η_{COL} is sensitive to d up to much larger d/L values, since the electron generation profile is biased towards the counter electrode side and responds effectively to changes in d. Due to these characteristics, comparison of spectral η_{IPCE} measurements taken at opposite illumination directions is a sensitive diagnostic tool for detecting inefficient electron collection[28,37,38].

APPENDIX B: Methods for the factorization of experimental η_{APCE} data into η_{INJ} and η_{COL} parts implied by the diffusion model

According to the diffusion model η_{APCE} is defined by four parameters: L, d, $\eta_{INJ}(\lambda)$ and $\alpha(\lambda)$ (eqs A2, A11, and A12). The characteristics of the model imply that if d and $\alpha(\lambda)$ are determined by independent measurements, analysis of the η_{APCE} data as a function of d, and the direction of illumination should enable factorization of η_{APCE} into its η_{INJ} and η_{COL} parts and estimating the steady state electron diffusion length L. In the following we use the diffusion model to formulate, besides the trivial case, two methods for this purpose.

The trivial case of 100 % η_{INJ} or η_{COL}

Decoupling η_{COL} and η_{INJ} is of course trivial if either η_{COL} or η_{INJ} (or both) is equal to 100 %. If η_{COL} can be assumed 100 %, η_{INJ} is given directly by the η_{APCE}, and vice versa. Relying only on η_{APCE} data, an experimental diagnostic of the condition $\eta_{COL} \approx 100$ % is that η_{APCE} is independent of the direction of illumination at strongly absorbed light wavelengths (see Figure 14).

Estimation of η_{INJ} by extrapolating η_{APCE} data to $d = 0$

The diffusion model predicts that the condition $\eta_{COL} \approx 100$ % is met when d is decreased until $d/L << 1$. Since L is unknown a priori, an estimate for η_{INJ} may be obtained by varying d experimentally and extrapolating η_{APCE} vs. d data to $d = 0$, under the assumption that L is independent of d. Due to the curvature in the η_{COL} vs. d/L relation in the region $d/L < 1$ (see Figure 14a) the method underestimates η_{INJ} slightly, at

most by 13 % for linear extrapolation, the error being smallest for strongly absorbed light incident from the PE side. With $\eta_{INJ}(\lambda)$ estimated, η_{COL} is readily obtained as $\eta_{COL}(\lambda,d) = \eta_{APCE}(\lambda,d)/\eta_{INJ}(\lambda)$, under the assumption that η_{INJ} is independent of d. Hence, η_{COL} follows the d-dependence of η_{APCE} but has in general different spectral shape. The method can be applied independently for both directions of illumination, and testing the reasonable expectation that $\eta_{INJ,PE}(\lambda) = \eta_{INJ,CE}(\lambda)$ may be used to assess the internal consistency of the data and the method. It is important to note that this method inherently assumes that the experimental η_{APCE} decreases systematically with d. Otherwise the condition $\eta_{COL} \approx 100$ % at $d = 0$ cannot be assumed.

Estimation of L based on the ratio of η_{APCE} at opposite illumination directions

The diffusion model implies that comparison of spectral η_{IPCE} data taken at opposite illumination directions provides not only a good diagnostic test for detecting low η_{COL} but also a method for quantitative estimation of L. According to the model, ratio $\eta_{APCE,CE}(\lambda,d)/\eta_{APCE,PE}(\lambda,d)$ depends only on $\alpha(\lambda)$, d and L, if $\eta_{INJ}(\lambda)$ can be assumed independent of the direction of illumination (cf. eqs A2, A11, and A12):

$$\frac{\eta_{APCE,CE}(\lambda,d)}{\eta_{APCE,PE}(\lambda,d)} = \frac{\eta_{COL,CE}(\lambda,d)}{\eta_{COL,PE}(\lambda,d)} = \frac{\sinh(d/L)+L\alpha(\lambda)\cosh(d/L)-L\alpha(\lambda)e^{\alpha(\lambda)d}}{\sinh(d/L)-L\alpha(\lambda)\cosh(d/L)+L\alpha(\lambda)e^{-\alpha(\lambda)d}}\cdot e^{-\alpha(\lambda)d}. \quad \text{(B1)}$$

Figure 14b demonstrates the high sensitivity of this ratio on d/L at constant L and α. In the limit of uniform light absorption ($1/\alpha >> d$), it equals unity, whereas in the limit of strongly absorbed light ($1/\alpha << d$), it equals to $\eta_{COL,CE}$ given by eq A14.

Using the experimental data for $\eta_{APCE,CE}/\eta_{APCE,PE}$, d, and $\alpha(\lambda)$, L can be estimated directly from eq B1 for each λ and d. With the estimated $L(\lambda,d)$, η_{COL} can be calculated from eqs A11-A12, and η_{INJ} subsequently as

$$\eta_{INJ}(\lambda,d)=\frac{\eta_{APCE,PE}(\lambda,d)}{\eta_{COL,PE}(\lambda,d)}=\frac{\eta_{APCE,CE}(\lambda,d)}{\eta_{COL,CE}(\lambda,d)}, \tag{B2}$$

where $\eta_{APCE,PE}(\lambda,d)$ and $\eta_{APCE,CE}(\lambda,d)$ are the experimental data. Hence, $\eta_{INJ}(\lambda)$ can be estimated independently for each d. The latter equality in eq B2 holds by definition since in this method, η_{INJ} is assumed independent of the illumination direction.

In contrast to the above extrapolation method, this method has the advantage that the decoupling of $\eta_{INJ}(\lambda)$ and $\eta_{COL}(\lambda)$ is in principle achieved without experimental variation of d. However, as demonstrated in the present paper, variation of d provides a necessary test for the validation of the data against the reasonable expectation that η_{INJ} is independent of d. While this method assumes that L is independent of the illumination direction no assumptions are made on the d-dependence of L.

References

(1) O'Regan, B.; Grätzel, M. *Nature* **1991***, 353*, 737-740.

(2) Peter, L. M. *Phys. Chem. Chem. Phys.* **2007***, 9*, 2630-2642.

(3) Nazeeruddin, M. K.; Kay, A.; Rodicio, I.; Humphry-Baker, R.; Müller, E.; Liska, P.; Vlachopoulos, N.; Grätzel, M. *J. Am. Chem. Soc.* **1993***, 115*, 6382-6390.

(4) Ito, S.; Nazeeruddin, K.; Liska, P.; Comte, P.; Charvet, R.; Pechy, P.; Jirousek, M.; Kay, A.; Zakeeruddin, S. M.; Grätzel, M. *Prog. Photovoltaics* **2006***, 14*, 589-601.

(5) Sommeling, P. M.; Späth, M.; Smit, H. J. P.; Bakker, N. J.; Kroon, J. M. *J. Photochem. Photobiol., A* **2004***, 164*, 137-144.

(6) Kroon, J. M.; Bakker, N. J.; Smit, H. J. P.; Liska, P.; Thampi, K. R.; Wang, P.; Zakeeruddin, S. M.; Grätzel, M.; Hinsch, A.; Hore, S.; Würfel, U.; Sastrawan, R.; Durrant, J. R.; Palomares, E.; Pettersson, H.; Gruszecki, T.; Walter, J.; Skupien, K.; Tulloch, G. E. *Prog. Photovoltaics* **2007***, 15*, 1-18.

(7) Kuang, D.; Klein, C.; Ito, S.; Moser, J.; Humphry-Baker, R.; Evans, N.; Duriaux, F.; Grätzel, C.; Zakeeruddin, S. M.; Grätzel, M. *Adv. Mater.* **2007***, 19*, 1133-1137.

(8) Kubo, W.; Sakamoto, A.; Kitamura, T.; Wada, Y.; Yanagida, S. *J. Photochem. Photobiol., A* **2004***, 164*, 33-39.

(9) Wang, Z.; Kawauchi, H.; Kashima, T.; Arakawa, H. *Coord. Chem. Rev.* **2004/7***, 248*, 1381-1389.

(10) Barbe, C. J.; Arendse, F.; Comte, P.; Jirousek, M.; Lenzmann, F.; Shklover, V.; Gratzel, M. *J. Am. Ceram. Soc.* **1997***, 80*, 3157-3171.

(11) Durrant, J. R.; Haque, S. A.; Palomares, E. *Coord. Chem. Rev.* **2004***, 248*, 1247-1257.

(12) Watson, D. F.; Meyer, G. J. *Coord. Chem. Rev.* **2004***, 248*, 1391-1406.

(13) Haque, S. A.; Palomares, E.; Cho, B. M.; Green, A. N. M.; Hirata, N.; Klug, D. R.; Durrant, J. R. *J. Am. Chem. Soc.* **2005***, 127*, 3456-3462.

(14) Lee, K.; Suryanarayanan, V.; Ho, K.; Justin Thomas, K. R.; Lin, J. T. *Sol. Energy Mater. Sol. Cells* **2007***, 91*, 1426-1431.

(15) Kusama, H.; Kurashige, M.; Arakawa, H. *J. Photochem. Photobiol., A* **2005***, 169*, 169-176.

(16) Kay, A.; Grätzel, M. *Chem. Mater.* **2002***, 14*, 2930-2935.

(17) Kumara, G. R. R. A.; Tennakone, K.; Perera, V. P. S.; Konno, A.; Kaneko, S.; Okuya, M. *J. Phys. D: Appl. Phys.* **2001***, 34*, 868-873.

(18) Sayama, K.; Sugihara, H.; Arakawa, H. *Chem. Mater.* **1998***, 10*, 3825-3832.

(19) Lana-Villarreal, T.; Boschloo, G.; Hagfeldt, A. *J. Phys. Chem. C* **2007***, 111*, 5549-5556.

(20) Lindström, H.; Holmberg, A.; Magnusson, E.; Lindquist, S.; Malmqvist, L.; Hagfeldt, A. *Nano Lett.* **2001***, 1*, 97-100.

(21) Hagfeldt, A.; Boschloo, G.; Lindström, H.; Figgemeier, E.; Holmberg, A.; Aranyos, V.; Magnusson, E.; Malmqvist, L. *Coord. Chem. Rev.* **2004***, 248*, 1501-1509.

(22) Miyasaka, T.; Kihirori, Y.; Ikegami, M. *Electrochemistry* **2007***, 75*, 2-12.

(23) Tachibana, Y.; Hara, K.; Sayama, K.; Arakawa, H. *Chem. Mater.* **2002***, 14*, 2527-2535.

(24) Quintana, M.; Edvinsson, T.; Hagfeldt, A.; Boschloo, G. *J. Phys. Chem. C* **2007***, 111*, 1035-1041.

(25) Heimer, T. A.; Heilweil, E. J.; Bignozzi, C. A.; Meyer, G. J. *J. Phys. Chem. A* **2000***, 104*, 4256-4262.

(26) Yanagida, M.; Yamaguchi, T.; Kurashige, M.; Hara, K.; Katoh, R.; Sugihara, H.; Arakawa, H. *Inorg. Chem.* **2003***, 42*, 7921-7931.

(27) O'Regan, B.; Moser, J.; Anderson, M.; Grätzel, M. *J. Phys. Chem.* **1990***, 94*, 8720-8726.

(28) Södergren, S.; Hagfeldt, A.; Olsson, J.; Lindquist, S. *J. Phys. Chem.* **1994***, 98*, 5552-5556.

(29) Lindström, H.; Magnusson, E.; Holmberg, A.; Södergren, S.; Lindquist, S.; Hagfeldt, A. *Sol. Energy Mater. Sol. Cells* **2002***, 73*, 91-101.

(30) Papageorgiou, N.; Maier, W. F.; Grätzel, M. *J. Electrochem. Soc.* **1997***, 144*, 876-884.

(31) Keis, K.; Roos, A. *Opt. Mater.* **2002***, 20*, 35-42.

(32) Dittrich, T.; Ofir, A.; Tirosh, S.; Grinis, L.; Zaban, A. *Appl. Phys. Lett.* **2006***, 88*, 182110/1-182110/3.

(33) Hore, S.; Vetter, C.; Kern, R.; Smit, H.; Hinsch, A. *Sol. Energy Mater. Sol. Cells* **2006***, 90*, 1176-1188.

(34) Hagfeldt, A.; Boschloo, G.; Lindström, H.; Figgemeier, E.; Holmberg, A.; Aranyos, V.; Magnusson, E.; Malmqvist, L. *Coord.Chem.Rev.* **2004**, *248*, 1501-1509.

(35) Lindström, H.; Holmberg, A.; Magnusson, E.; Malmqvist, L.; Hagfeldt, A. *J. Photochem. Photobiol., A* **2001***, 145*, 107-112.

(36) Halme, J.; Saarinen, J.; Lund, P. *Sol. Energy Mater. Sol. Cells* **2006***, 90*, 887-899.

(37) Lindström, H.; Rensmo, H.; Södergren, S.; Solbrand, A.; Lindquist, S. *J. Phys. Chem.* **1996***, 100*, 3084-3088.

(38) Boschloo, G. K.; Goossens, A. *J. Phys. Chem.* **1996***, 100*, 19489-19494.

(39) Peter, L. M.; Wijayantha, K. G. U. *Electrochem. Commun.* **1999***, 1*, 576-580.

(40) Fisher, A. C.; Peter, L. M.; Ponomarev, E. A.; Walker, A. B.; Wijayantha, K. G. U. *J. Phys. Chem. B* **2000***, 104*, 949-958.

(41) Trupke, T.; Würfel, P.; Uhlendorf, I. *J. Phys. Chem. B* **2000***, 104*, 11484-11488.

(42) Zhang, Z.; Zakeeruddin, S. M.; O'Regan, B. C.; Humphry-Baker, R.; Grätzel, M. *J. Phys. Chem. B* **2005***, 109*, 21818-21824.

(43) Rühle, S.; Greenshtein, M.; Chen, S. -.; Merson, A.; Pizem, H.; Sukenik, C. S.; Cahen, D.; Zaban, A. *J. Phys. Chem. B* **2005***, 109*, 18907-18913.

(44) Neale, N. R.; Kopidakis, N.; van de Lagemaat, J.; Grätzel, M.; Frank, A. J. *J. Phys. Chem. B* **2005***, 109*, 23183-23189.

(45) Kelly, C. A.; Farzad, F.; Thompson, D. W.; Stipkala, J. M.; Meyer, G. J. *Langmuir* **1999***, 15*, 7047-7054.

(46) Qu, P.; Meyer, G. J. *Langmuir* **2001***, 17*, 6720-6728.

(47) Hara, K.; Horiguchi, T.; Kinoshita, T.; Sayama, K.; Arakawa, H. *Sol. Energy Mater. Sol. Cells* **2001***, 70*, 151-161.

(48) Fukui, A.; Komiya, R.; Yamanaka, R.; Islam, A.; Han, L. *Sol. Energy Mater. Sol. Cells* **2006***, 90*, 649-658.

(49) Zaban, A.; Ferrere, S.; Gregg, B. A. *J. Phys. Chem. B* **1998***, 102*, 452-460.

(50) Katoh, R.; Furube, A.; Murai, M.; Tamaki, Y.; Hara, K.; Tachiya, M. *C. R. Chimie* **2006***, 9*, 639-644.

(51) Moser, J.; Grätzel, M. *Chimia* **1998***, 52*, 160-162.

(52) Boschloo, G.; Lindström, H.; Magnusson, E.; Holmberg, A.; Hagfeldt, A. *J. Photochem. Photobiol., A* **2002***, 148*, 11-15.

(53) Anderson, N. A.; Lian, T. *Coord. Chem. Rev.* **2004***, 248*, 1231-1246.

(54) Lenzmann, F.; Krueger, J.; Burnside, S.; Brooks, K.; Grätzel, M.; Gal, D.; Rühle, S.; Cahen, D. *J. Phys. Chem. B* **2001***, 105*, 6347-6352.

(55) Altobello, S.; Argazzi, R.; Caramori, S.; Contado, C.; Da Fre, S.; Rubino, P.; Chone, C.; Larramona, G.; Bignozzi, C. A. *J. Am. Chem. Soc.* **2005***, 127*, 15342-15343.

(56) Benkstein, K. D.; Kopidakis, N.; Van De Lagemaat, J.; Frank, A. J. *Mater. Res. Soc. Symp. Proc.* **2004***, 789*, 325-330.

(57) van de Lagemaat, J.; Benkstein, K. D.; Frank, A. J. *J. Phys. Chem. B* **2001***, 105*, 12433-12436.

(58) Cao, F.; Oskam, G.; Meyer, G. J.; Searson, P. C. *J. Phys. Chem.* **1996***, 100*, 17021-17027.

(59) de Jongh, P. E.; Vanmaekelbergh, D. *Phys. Rev. Lett.* **1996***, 77*, 3427-3430.

(60) Bisquert, J.; Vikhrenko, V. S. *J. Phys. Chem. B* **2004***, 108*, 2313-2322.

(61) Anta, J. A.; Casanueva, F.; Oskam, G. *J. Phys. Chem. B* **2006***, 110*, 5372-5378.

(62) Boschloo, G.; Hagfeldt, A. *J. Phys. Chem. B* **2005**, *109*, 12093-12098

(63) Lobato, K.; Peter, L. M.; Würfel, U. *J. Phys. Chem. B* **2006***, 110*, 16201-16204.

(64) Würfel, U.; Wagner, J.; Hinsch, A. *J. Phys. Chem. B* **2005***, 109*, 20444-20448.

(65) Cameron, P. J.; Peter, L. M. *J. Phys. Chem. B* **2003***, 107*, 14394-14400.

(66) Bay, L.; West, K.; Winther-Jensen, B.; Jacobsen, T. *Sol. Energy Mater. Sol. Cells* **2006***, 90,* 341-351

(67) Cameron, P. J.; Peter, L. M.; Hore, S. *J. Phys. Chem. B* **2005***, 109*, 930-936.

(68) Ito, S.; Liska, P.; Comte, P.; Charvet, R.; Pechy, P.; Bach, U.; Schmidt-Mende, L.; Zakeeruddin, S. M.; Kay, A.; Nazeeruddin, M. K.; Grätzel, M. *Chem. Commun.* **2005**, 4351-4353.

(69) Hore, S.; Kern, R. *Appl. Phys. Lett.* **2005***, 87*, 263504/1-263504/3.

(70) Xia, J.; Masaki, N.; Jiang, K.; Yanagida, S. *J. Phys. Chem. C* **2007***, 111*, 8092-8097.

(71) Xia, J.; Masaki, N.; Jiang, K.; Yanagida, S. *J. Photochem. Photobiol., A* **2007***, 188*, 120-127.

(72) Xia, J.; Masaki, N.; Jiang, K.; Yanagida, S. *J. Phys. Chem. B* **2006***, 110*, 25222-25228.

(73) Liu, X.; Huang, Z.; Li, K.; Li, H.; Li, D.; Chen, L.; Meng, Q. *Chin. Phys. Lett.* **2006***, 23*, 2606-2608.

(74) Maheu, B.; Gouesbet, G. *Appl. Opt.* **1986***, 25*, 1122-1128.

(75) Rothenberger, G.; Comte, P.; Grätzel, M. *Sol. Energy Mater. Sol. Cells* **1999/7/15***, 58*, 321-336.

(76) Papageorgiou, N.; Grätzel, M.; Infelta, P. P. *Sol. Energy Mater. Sol. Cells* **1996***, 44*, 405-438.

(77) Papageorgiou, N.; Liska, P.; Kay, A.; Grätzel, M. *J. Electrochem. Soc.* **1999***, 146*, 898-907.

(78) Papageorgiou, N.; Athanassov, Y.; Armand, M.; Bonhôte, P.; Pettersson, H.; Azam, A.; Grätzel, M. *J. Electrochem. Soc.* **1996***, 143*, 3099-3108.

Figure Captions

Figure 1. Photocurrent determining processes in DSC. With a probability η_{LH} a photon incident on the cell generates an exited state in a dye molecule (1). For high η_{INJ}, electron injection to TiO_2 conduction band (2) needs to be faster than radiationless relaxation (a), and dye regeneration (3) needs to be faster than electron recombination with the oxidized dye (b). After successful injection the electron is released to transport in TiO_2 nanoparticle film (4). With a probability η_{COL} it avoids recombination with electrolyte species (c) and is measured as a photocurrent in the external electric circuit.

Figure 2. Relation between TiO_2 film porosity and thickness (d) after final compression. The error limits are based on uncertainties in film volume (2 - 9 %) and mass (5 μg accuracy). The latter dominates in the thin films constituting at most 50 % of the total uncertainty. The inset shows a typical cross-section profile of a pressed TiO_2 film.

Figure 3. Optical characteristics and η_{LH}: (a-c) the reflectance (R), transmittance (T) and absorptance (A) of dyed TiO_2 films. The arrows indicate increasing film thickness; (d) transmittance of free electrolyte layer (T_{EL}, thickness 23 μm), photoelectrode substrate (T_{FTO}), and counter electrode (T_{CE}); (e-f) the effect of film thickness and illumination direction on η_{LH} calculated from the optical data.

Figure 4. Short circuit current density (i_{SC}) and energy conversion efficiency (η) at 100 mW/cm^2 light intensity. The error bars indicate average roughness within FWHM of the film profile and standard deviation of i_{SC}. The lines are guides to the eye.

Figure 5. η_{IPCE} of the P cells. Effect of light wavelength (λ), film thickness (d) and direction of illumination on η_{IPCE}: (a-c) at PE side illumination, (e-f) at CE side illumination. (a,d): average data for each d-group; (b,e): η_{IPCE} vs. d at λ = 535 nm, 640 nm and 700 nm. The lines are 2nd order polynomial fits to the data; (c,f): normalized η_{IPCE} spectra. Individual data (2-3 samples per d-group).

Figure 6. η_{IPCE} of the S cells. See Figure 5 for descriptions.

Figure 7. η_{IPCE} as a function of light intensity at λ = 639 nm for different number of TiO_2 layers: (a) P cells; (b) S cells.

Figure 8. η_{APCE} of the P cells. Effect of light wavelength (λ), film thickness (d) and direction of illumination on η_{APCE}: (a-c) at PE side illumination, (e-f) at CE side illumination. (a,d): average data for each d-group; (b,e): η_{APCE} vs. d at λ = 535 nm, 640 nm and 700 nm. The lines are 2nd order polynomial fits to the data; (c,f): normalized η_{APCE} spectra. Individual data (2-3 samples per d-group).

Figure 9. η_{APCE} of the S cells. See Figure 8 for descriptions.

Figure 10. Spectral η_{APCE} extrapolated to d = 0 at each λ by 2nd order polynomial fit to the η_{APCE} vs. d data (as in Figures 8b,e and 9b,e). The error bars indicate 50 % confidence interval assuming independent and normal errors with constant variance. The inset shows the normalized spectra. CE side data for the P cells is omitted, since the extrapolation is unreliable due to strong d-dependence at the short wavelengths (cf. Figure 5e).

Figure 11. Spectral η_{COL} of the P cells estimated by the extrapolation method. Average experimental data and calculated model data by fitting at λ = 535 nm at (a) PE illumination and (b) CE illumination, for different number of TiO_2 layers.

Figure 12. Application of the η_{APCE} ratio method to the S cells. (a) experimental $\eta_{APCE,CE}/\eta_{APCE,PE}$ data; (b) L and (c) η_{INJ}, estimated by eqs B1 and B2 using experimental values for d, α, and $\eta_{APCE,CE}/\eta_{APCE,PE}$.

Figure 13. The estimated effective electron diffusion (L) length as a function of the photoelectrode film thickness (d) for the S and P cells. Open symbols: L based on the extrapolation method; Filled symbols: L based on the η_{APCE} ratio method. Note that $L/2$ is shown for the S cells. For the thickest S films, estimation of L becomes inaccurate for data points with η_{APCE} close to the η_{INJ}, yielding too large L estimates. These data are excluded from the figure.

Figure 14. Characteristics of the diffusion model for constant L and α. (a) electron collection efficiency (eqs A9-A12) and (b) ratio $\eta_{COL,CE}/\eta_{COL,PE}$ as function of d/L (eq 2). The arrows in (a) show the direction of increasing optical penetration depth $1/\alpha$ compared to the diffusion length L.

Figures

Figure 1

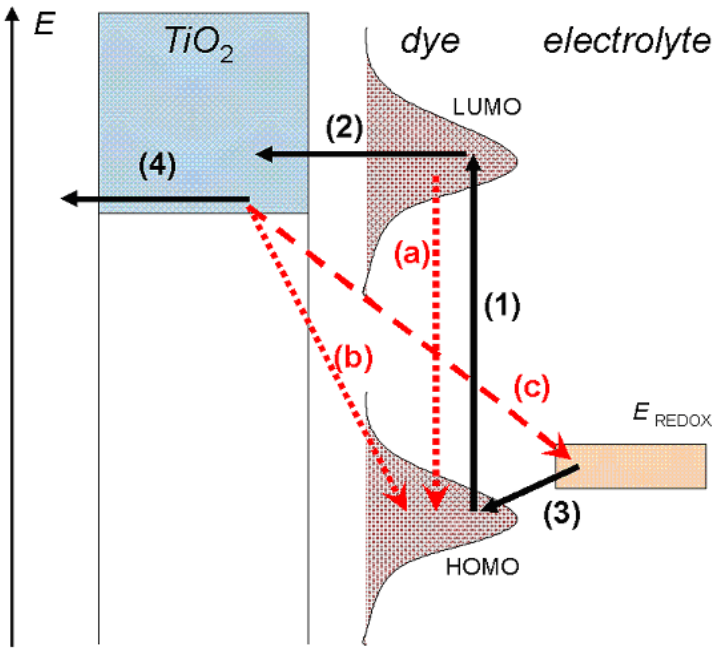

Figure 2

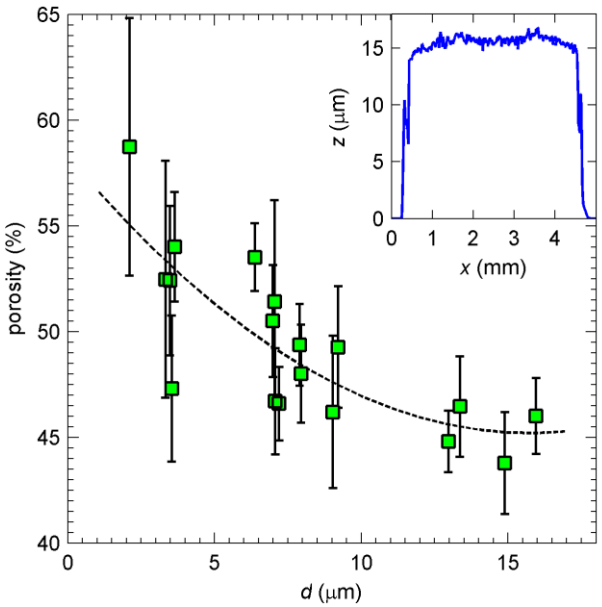

Figure 3

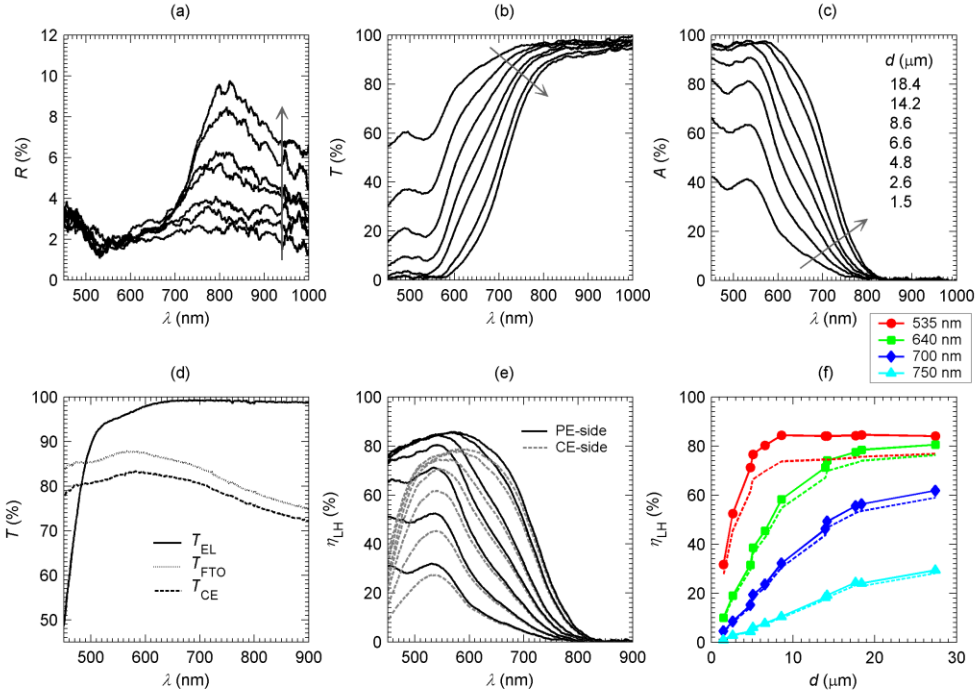
(a)
(b)
(c)
(d)
(e)
(f)
R (%)
T (%)
A (%)
λ (nm)
d (μm)
18.4
14.2
8.6
6.6
4.8
2.6
1.5
535 nm
640 nm
700 nm
750 nm
T_EL
T_FTO
T_CE
PE-side
CE-side
η_LH (%)

Figure 4

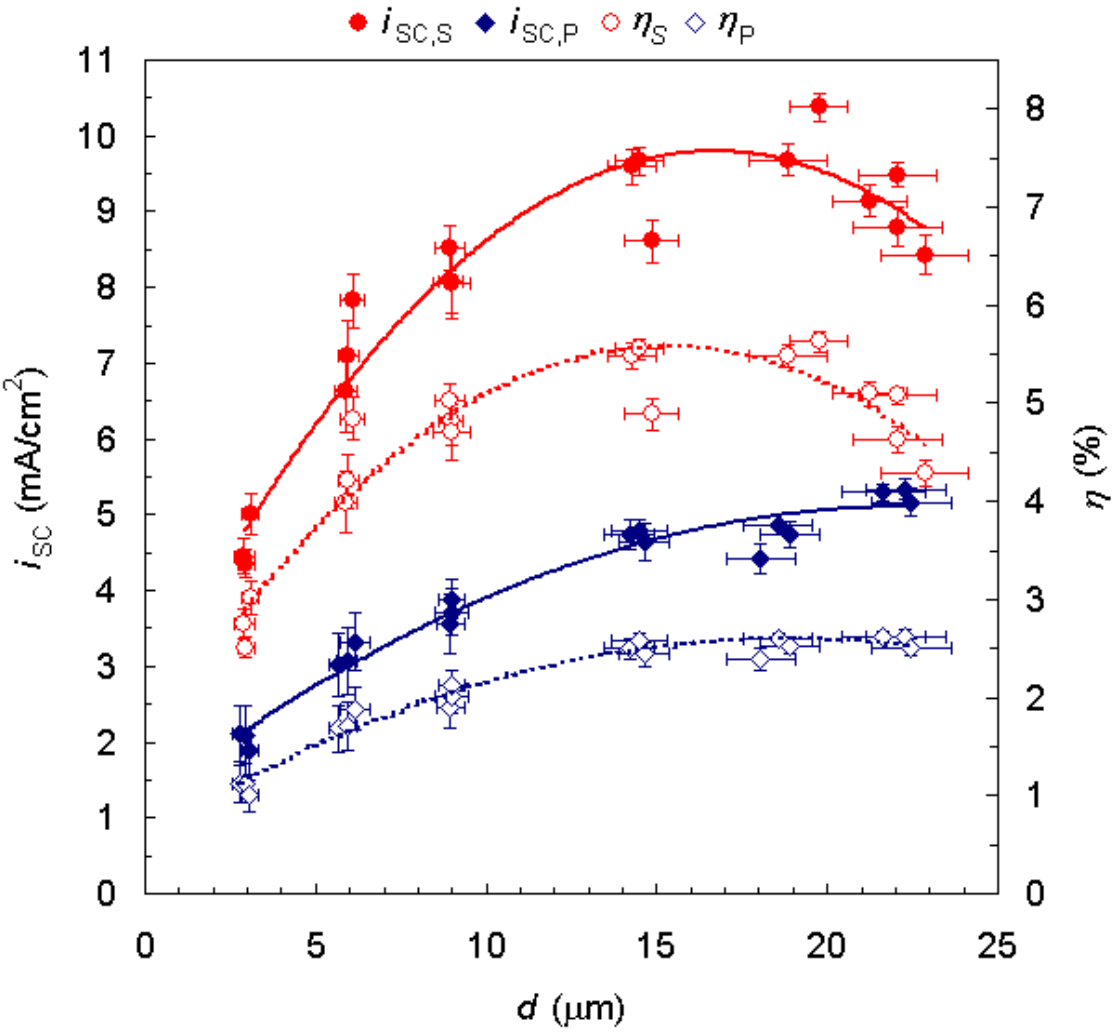
$i_{SC,S}$ $i_{SC,P}$ η_S η_P
i_{SC} (mA/cm^2)
η (%)
d (μm)
0
1
2
3
4
5
6
7
8
9
10
11
0
5
10
15
20
25

Figure 5

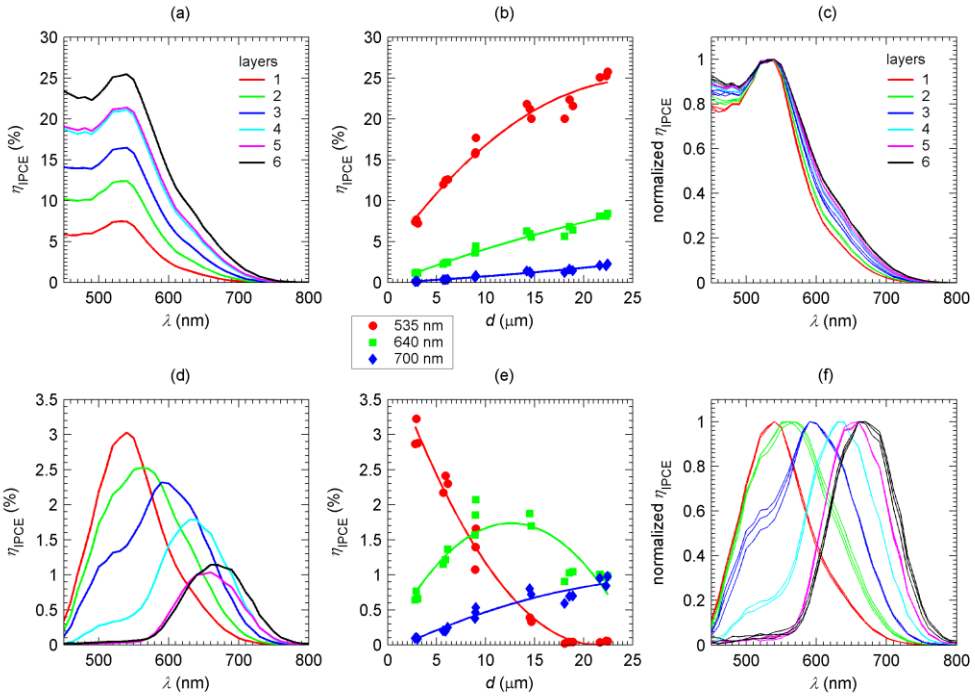

Figure 6

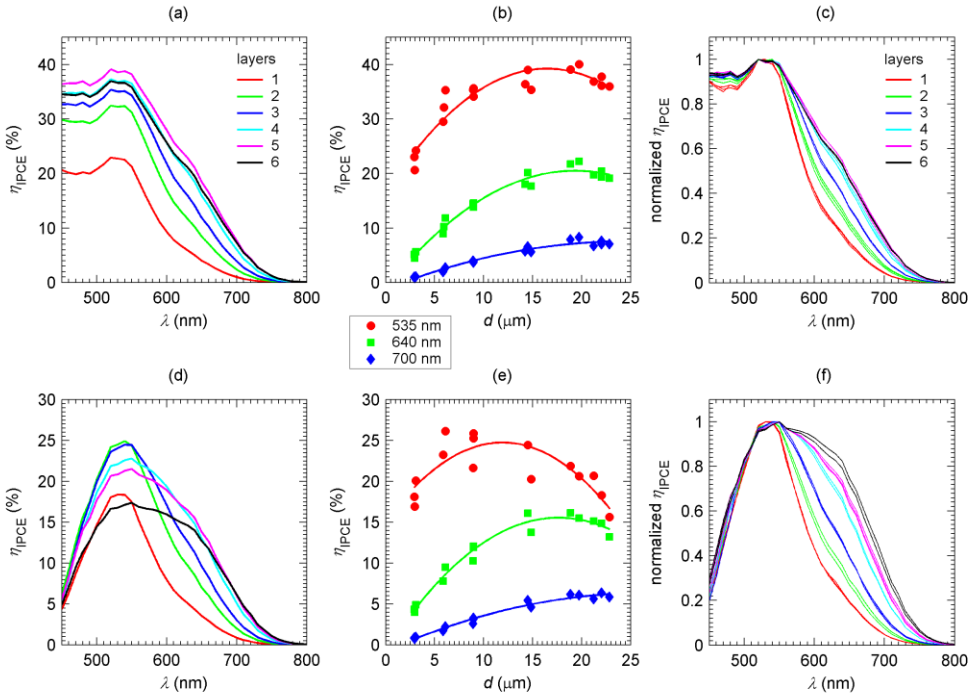

Figure 7

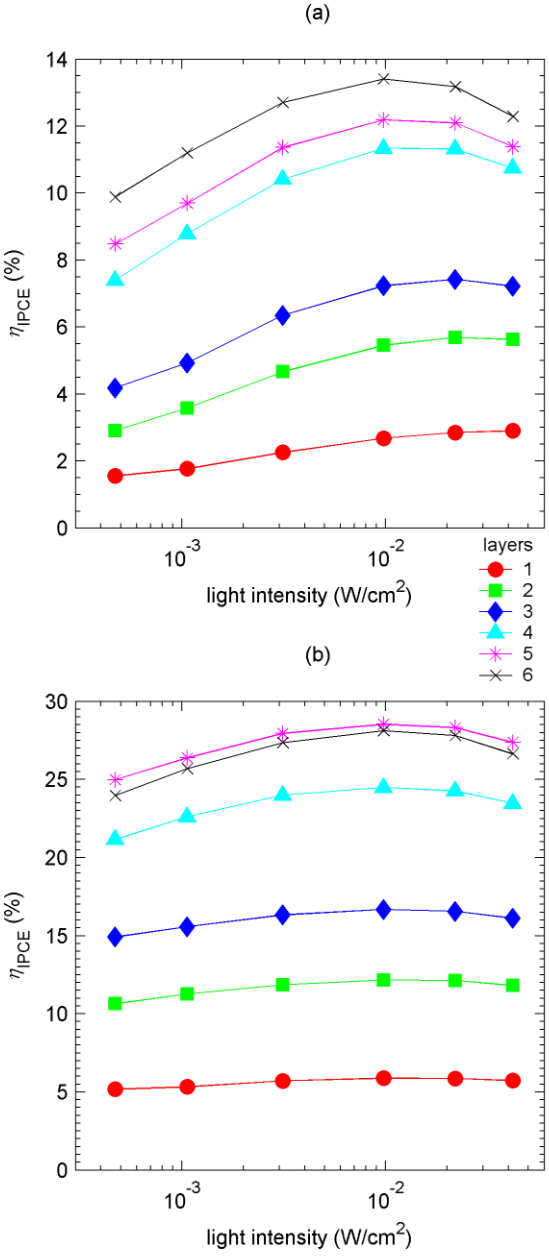
(a)
η_{IPCE} (%)
light intensity (W/cm^2)
layers
1
2
3
4
5
6
(b)
η_{IPCE} (%)
light intensity (W/cm^2)

Figure 8

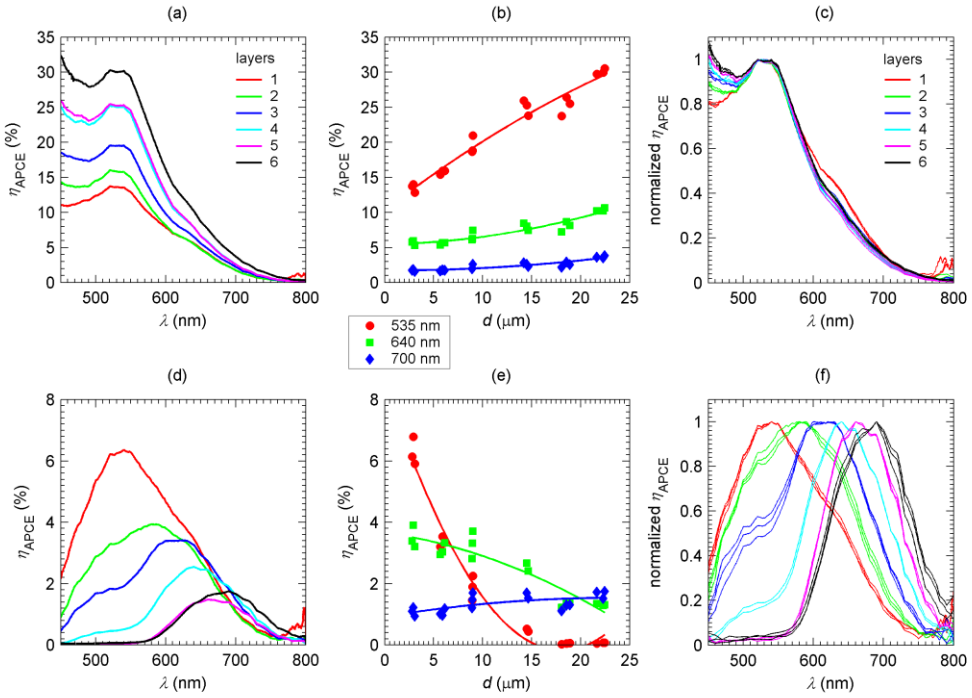

Figure 9

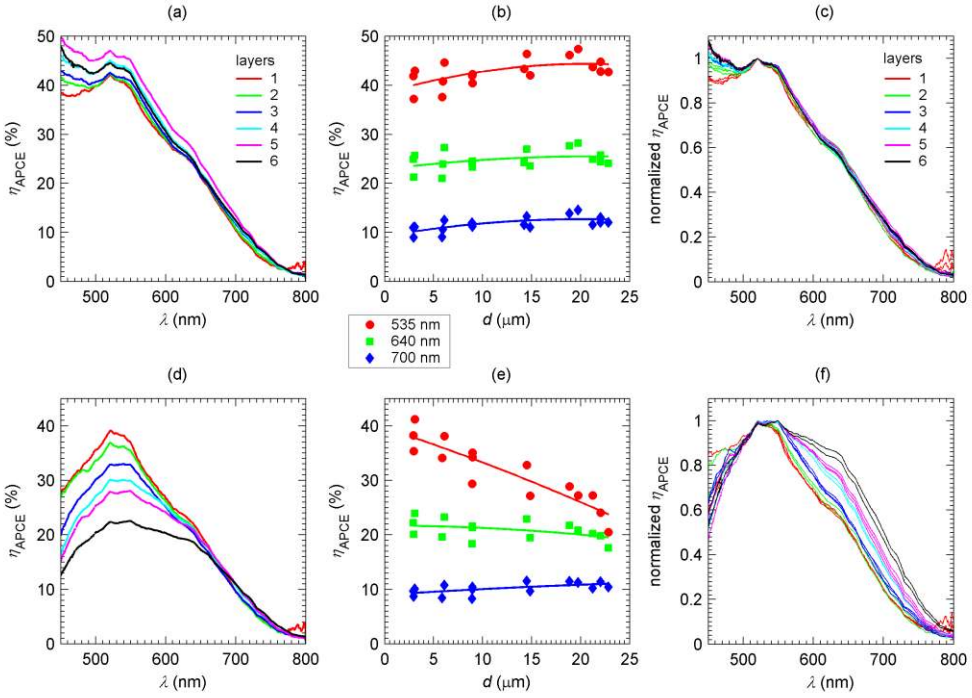

Figure 10

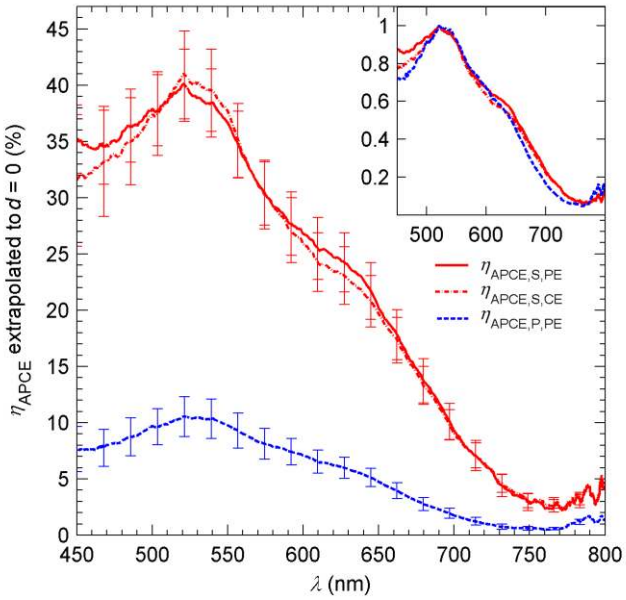
η_{APCE} extrapolated to d = 0 (%)
λ (nm)
$\eta_{APCE,S,PE}$
$\eta_{APCE,S,CE}$
$\eta_{APCE,P,PE}$

Figure 11

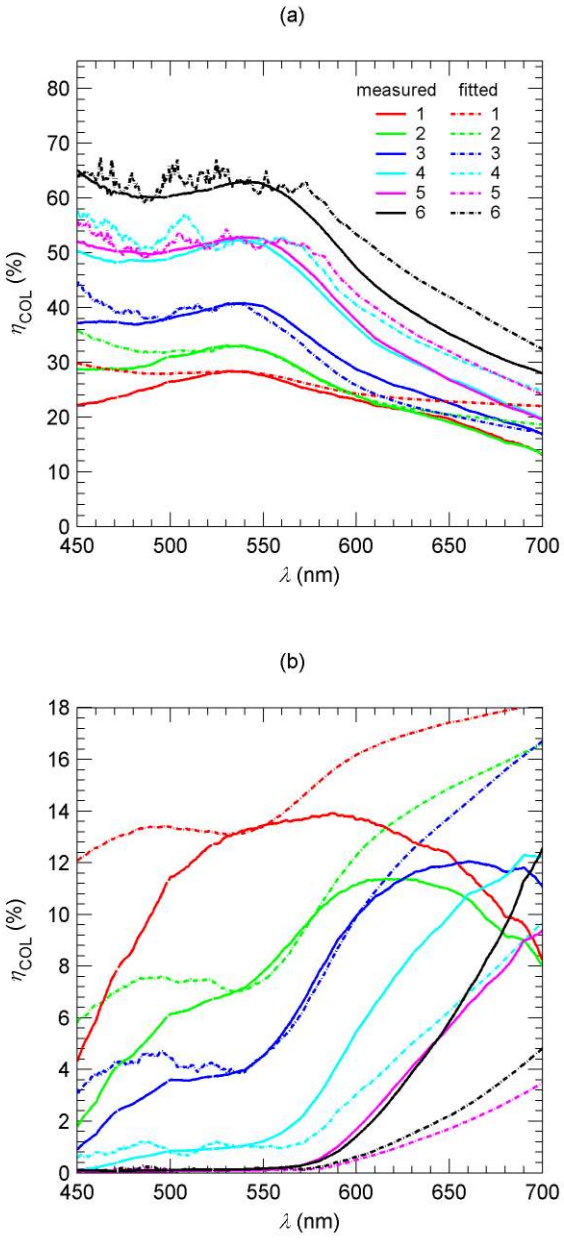
(a)
measured
fitted
1
2
3
4
5
6
η_{COL} (%)
λ (nm)
(b)
η_{COL} (%)
λ (nm)

Figure 12

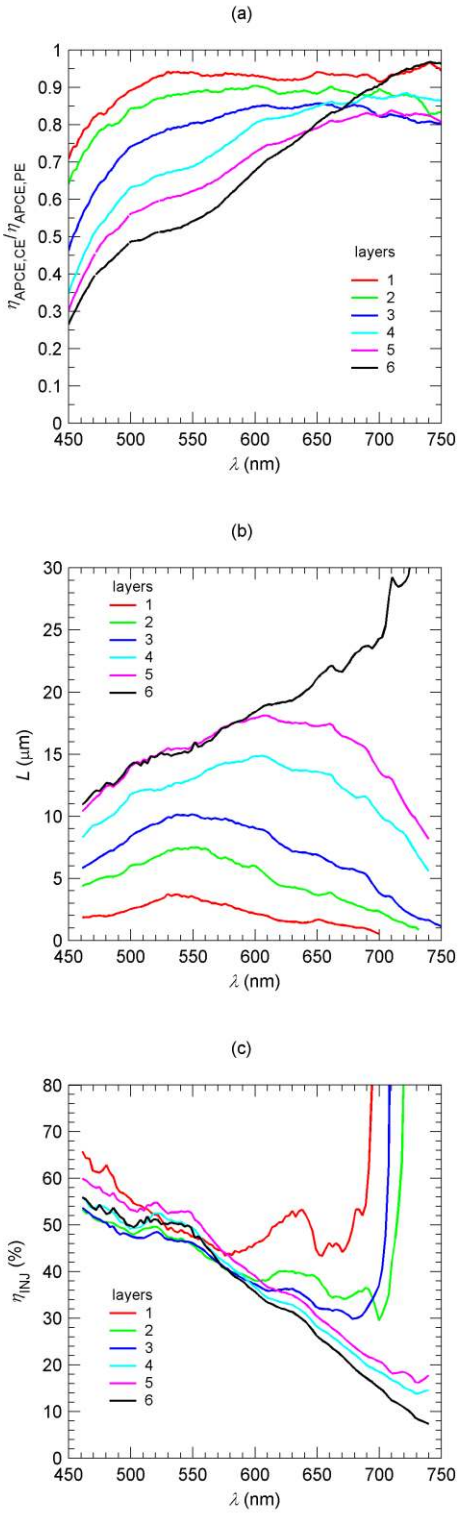
(a)
$\eta_{APCE,CE}/\eta_{APCE,PE}$
λ (nm)
layers
1
2
3
4
5
6
(b)
L (μm)
λ (nm)
layers
1
2
3
4
5
6
(c)
η_{INJ} (%)
λ (nm)
layers
1
2
3
4
5
6

Figure 13

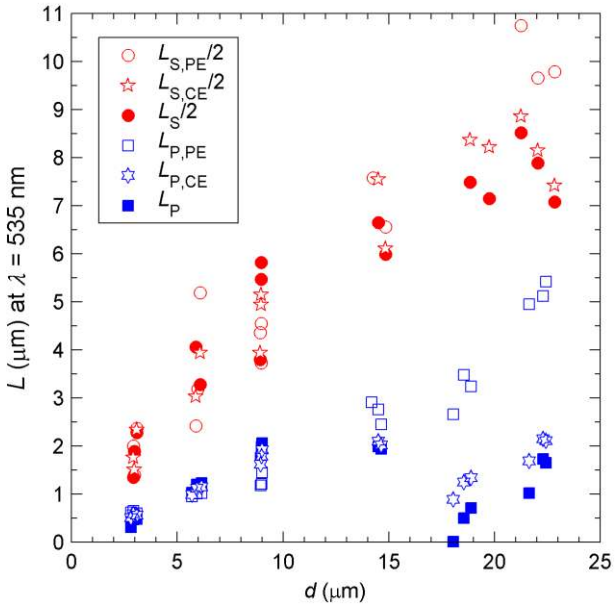
$L_{S,PE}/2$
$L_{S,CE}/2$
$L_S/2$
$L_{P,PE}$
$L_{P,CE}$
L_P
L (μm) at λ = 535 nm
d (μm)
0
1
2
3
4
5
6
7
8
9
10
11
0
5
10
15
20
25

Figure 14

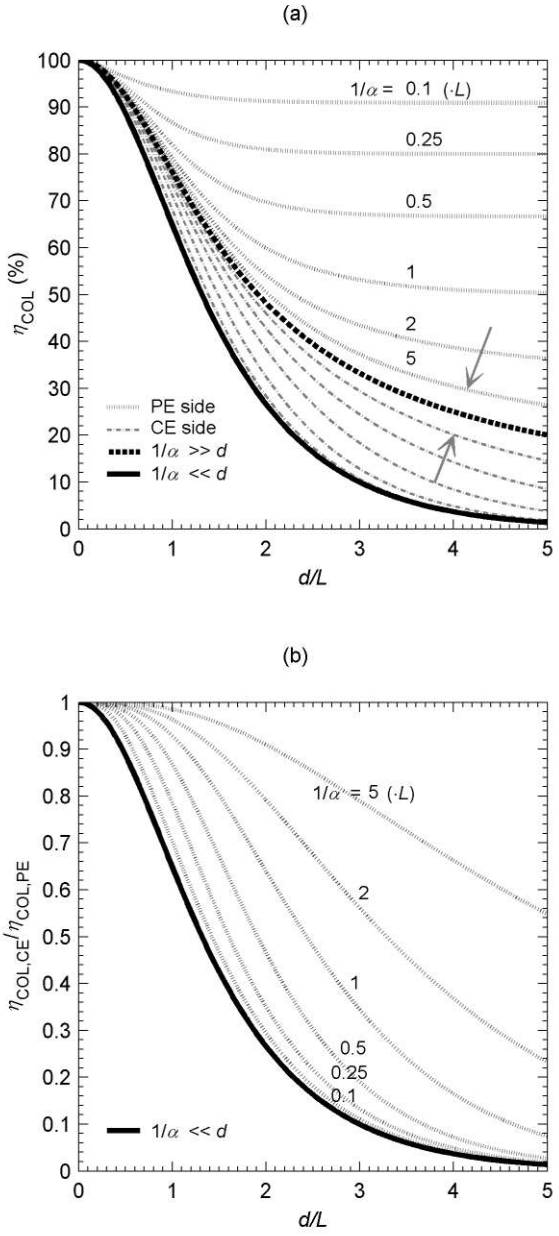
(a)
100
90
80
70
60
50
40
30
20
10
0
0
1
2
3
4
5
η_{COL} (%)
d/L
1/α = 0.1 (·L)
0.25
0.5
1
2
5
PE side
CE side
1/α >> d
1/α << d
(b)
1
0.9
0.8
0.7
0.6
0.5
0.4
0.3
0.2
0.1
0
0
1
2
3
4
5
$\eta_{COL,CE}/\eta_{COL,PE}$
d/L
1/α = 5 (·L)
2
1
0.5
0.25
0.1
1/α << d